Using Computational Fluid Dynamics for Evaluating the Pollutant Formation in a Biomass Pellet Burner

Anthony Durbano

A thesis submitted for the degree of
Laurea Magistrale in
Energy Engineering for an Environmentally
Sustainable World
at Politecnico di Milano

July 2015

Except where otherwise indicated, this thesis is my own original work.

Anthony Durbano

14 July 2015

Acknowledgements

A special thanks to Enrique Chacón Tanarro and the entire Departamento de Ingeniería Mecánica at the Universidad Politécnica de Madrid

Abstract

The following report contains a CFD analysis for determining the optimal design and operation of an existing grate burner prototype created in the Departamento de Ingeniería Mecánica at the Universidad Politécnica de Madrid. The current design consists of a combustion chamber and an antechamber, and is fed primary air from underneath the grate and secondary air horizontally over the pellet pile. A comprehensive model of the prototype was created, consisting of three scales: the pellet scale, the pellet-pile scale, and the entire-burner scale. Considering each of these scales quasi-independently, the model was used to predict the outcome of different modifications on the operation and degisn. It was determined that CO and NO_x emissions can be significantly reduced after certain modifications are made to how the existing burner is constructed and operated. The results of this study will be incorporated into future prototypes.

Contents

List of Figures

Chapter 1

Introduction

1.1 Global warming and its effect on energy production

With the current advent of rising global temperatures, extreme weather phenomena, and melting ice caps, occurring at rates not paralleled since the first collections of meteorological data, the presence of global warming has become clear. This warming comes in tandem with the industrial revolution and the proliferation of fossil fuel use. Since these trends coincide quite closely with respect to time, the culpability of global warming is also becoming increasingly clear.

The so-called *greenhouse effect* predicts that an increased presence of certain gaseous compounds in Earth's atmosphere inhibits the planet's ability to reject solar heat. One of the most significant of these compounds, due to its abundance, is CO_2 [8]. Since CO_2 is one of the two major products of all combustion-based energy generation, it is apparent that the increased energy demand of the human race is directly contributing to the global warming effect.

Now that recognition of this scientific consensus has become more widespread, the necessity to curtail CO_2 emissions is much more accepted by the general populace in most modernized countries, to the point that global warming is now affecting public policy. The European Union, for example, has implemented a policy called "20-20-20" with the following goals [5]:

1. Reducing the EU greenhouse gas emissions to levels before 1990
2. Raising the share of energy consumption to come from 20% renewable energy
3. A 20% improvement of the EU's overall energy efficiency

Broad-reaching policies such as this require countries to diversify their energy portfolios to include many energy sources, placing a heavy preference toward the development of *CO_2-neutral energy sources*[1]. Such sources include:

[1] CO_2-neutral energy source: an energy source that, during its entire lifetime including collection and energy extraction, has a net CO_2 emission of zero or less

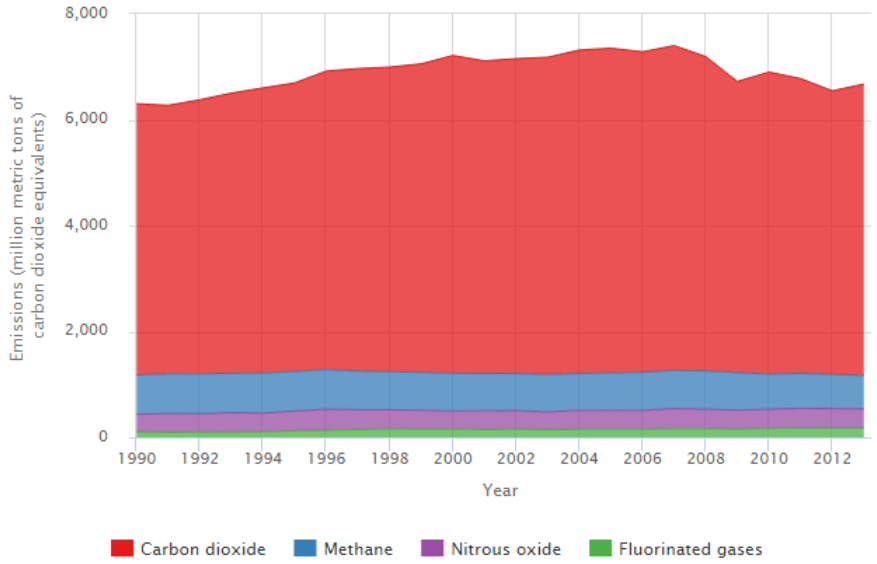

Figure 1.1: U.S. Greenhouse Gas Emissions by Gas, 1990-2013 [8]

- Solar Energy - Collected by means of photovoltaic cells or by solar-thermal collectors
- Wind Energy - Collected by wind turbines [45]
- Nuclear Energy - Collected from mainly uranium via various types of fission reactors [6]
- Hydro Energy - Collected from rivers and reservoirs using turbines
- Geothermal Energy - Collected using heat extraction wells, usually followed by a steam turbine
- Biomass Energy - Collected from any form of non-fossilized[2] biological material [45]

Depending on the availability of these sources, countries have developed very different portfolios. In the United States, due to its incredibly large agricultural industry, the largest CO_2-neutral energy source is biomass energy [1]. In countries that receive a great amount of solar radiation, especially those closer to the equator, such as Spain, the energy portfolios contain larger contributions from solar farms, either as photovoltaic cells or as solar-thermal collectors. In other countries, that do not have such resources readily available, a possible alternative is nuclear energy. France, for example, is able to produce more than 70% of its consumed energy from nuclear [7].

[2]Fossil fuels are considered differently from biomass because, on the timescale of human activity, the carbon contained in fossils has never been in the atmosphere, whereas the carbon in biomass has.

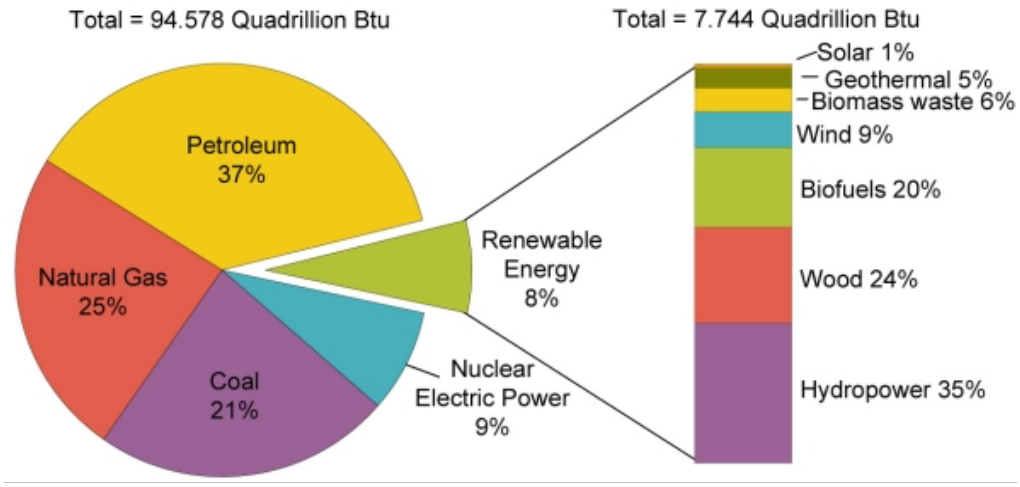

Figure 1.2: U.S. Energy Consumption by Source, 2009 [1]

Another great advantage of many renewable resources, from an energy distribution perspective, is the dispersion of energy generators. The original electrical grid, at the time it was first developed, depended on large power plants for generating electricity, followed by very expansive transmission systems to carry that electricity over great distances [46]. Maintaining this transmission system is expensive and can potentially make up about half of the purchase price of electricity [31]. With new, smaller energy generators ranging from wind farms to solar panels on a household roof, the new electricity paradigm is slowly shifting toward a higher share of *dispersed generation*[3]. This comes with added pitfalls, especially in predictability, but it has the huge advantage of consumers needing to withdrawal less of their energy from the electric grid, meaning cheaper energy prices in the long run [46].

In the same vein, residential heat generation, in many places such as Sweden, Denmark, or Austria, is also shifting toward a paradigm of local energy generation instead of relying on transmission systems of electricity or gas. *District heating*[4] creates a new demand for local heat generation, and one of the major energy sources used is biomass [36]. Biomass is a convenient energy source because it is a relatively cheap energy source that also requires relatively cheap equipment with respect to other renewable energy sources. Biomass also has the benefit of well developed combustion technologies that have been developed for centuries and even millennia. The focus of this study will be on these types of small scale biomass burners, which, due to the proliferation of these new heating solutions, are becoming more and more popular.

[3]Dispersed generation: power generators attached to the electrical grid at medium or low voltage levels on the distribution system

[4]heat generation and distribution for a group of residents on site or nearby

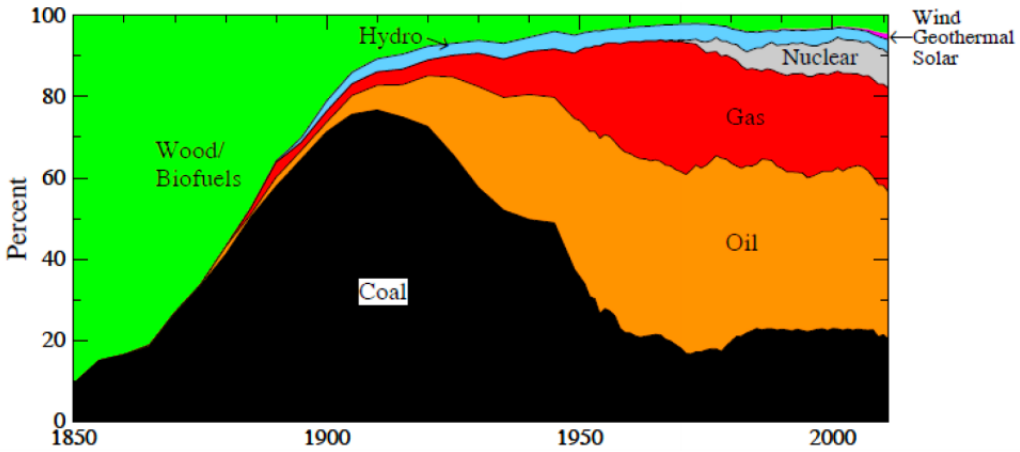

Figure 1.3: History of U.S. Primary Energy Consumption [19]

1.2 A brief history of biomass-derived energy and its viability as an energy source

Biomass, as an energy source, is not only ancient, but quite possibly the first energy source harnessed by humans for their own purposes. Anthropologists and archeologists note, based on historical evidence, that great advances of the human species came with the "discovery" of fire. Humans learned to take energy sources (mainly wood or grass), store them, and then elect to use them whenever they chose [45]. No longer was man dependent on nature to provide him heat or light. He could create them for himself.

It is this same concept which has driven much of human development since, especially in the wake of the Industrial Revolution. The industrial revolution exponentially decreased the demand of storing and using large quantities of energy all at once. The scale necessary for many of the works of the industrial age arose from the fact that energy was utilized in a much more concentrated fashion [47]. It was also this great energy demand that prompted the major energy source shift for the first time in thousands of years (see figure 1.3). Using coal as an energy source won out over the use of biomass because it was cheaper, faster, and more abundant [55]. The same is true today. Considering large-scale industrial operations, using biomass as an energy source still is not economically preferable to fossil fuels. Heavy research efforts are at work attempting to make it reality. McCarl et al. have studied the prospects of biomass, suggesting improvements in energy production, crop production, and shifting to short-rotation woody crops. However, the fact of the matter is, without incentives, on an industrial scale, biomass does not currently compete [32].

There are several alternatives to using biomass for energy that are more feasible technologically and economically. Biomass cofiring[5] with fossil fuels is a much more

[5]Cofiring: the burning of a mixture of fuel types; typically referring to a mixture of biomass and fossil fuels

cost-effective approach of integration into the energy industry on a large scale. Power generators are able to reduce their net CO_2 output and benefit from the incentives awarded for utilising biomass. Cofiring also has the intrinsic benefit of there already being existing plants which can be modified to handle mixed fuels. Initial research began in the 1980s. The first pilot plants in the U.S. went into operation in 1992, with the amount growing since then [49].

The more interesting niche for biomass, currently, is on the small-scale market, where biomass is making gains. On this level, biomass does not perform well in the case of electricity generation, but it has proven very useful for district or residential heating. In the case of district heating, new government incentives and production targets are leading to installation of new biomass district heating systems all over the world [36]. Again, thanks to less withdrawal from the electric grid or the gas pipeline, utilizing biomass could potentially save money in the long term. It also has the added bonus of reducing some of the major pollutants associated with fossil fuel burning, such as sulfuric acids. Since biomass has virtually no sulfur content, this problem is removed completely. Unfortunately, using biomass in the same burner technologies that are used for coal does present new problems that are biomass-specific.

1.3 Issues specific to biomass

Biomass is currently considered as a substitute or even a supplement to coal, in the cases where biomass is used as a direct energy source[6]. Therefore, any comparisons made between biomass and conventional fossil fuels will be specific to coal. Biomass has many major advantages over coal. To name a few:

- The carbon to be burned comes from sequestered CO_2 in the atmosphere (CO_2-neutral)
- Trace amounts of sulfur, leading to much lower emission of SO_x
- Less metal content, so less production of ash [56]

While many of the benefits of biomass are clear, the use of biomass also has its drawbacks, both from an industrial perspective and from a technical perspective. On the larger scale:

- Biomass production from wood requires deforestation or dedicated agricultural production

[6] As opposed to biomass' use as an indirect energy source if it is used to manufacture bioethanol or biodiesel

- Biomass production from other crops requires dedicated agricultural production
- The supply chain of biomass is subject to many variables [29]

And on the local operating scale:

- Biomass has a lower amount of energy (lower heating value) per mass
- Biomass has a higher moisture content, which limits flue gas temperatures
- Biomass has greater nitrogen content, leading to higher production of NO_x
- The lower heating leads to lower combustion efficiencies, meaning more CO
- More complex molecular structure leads to the release of more volatile organics [13]

As a result of these new problems, the combustion technology previously used for coal can prove to be unacceptable if emission limits are to be respected and if efficiency of the system is to be optimized. Therefore, several new solutions must be proposed to alleviate some of biomass' most significant drawbacks.

1.4 Current state of biomass technology and research

After the 1973 oil crisis, many western nations who relied on petroleum for energy generation were forced to explore different sources when the price of oil nearly quadrupled. Since the late 1970s, the International Energy Agency (IEA) has provided a framework for coordinating biomass research and technology developments. Countries involved (or previously involved) in this effort include Austria, Canada, Denmark, Finland, Italy, the Netherlands, Norway, Sweden, Switzerland, the UK, and the US. In 1994, the research areas organised by the IEA included:

- Characterisation of fuel and ash (Austria)
- Emissions from biomass combustion (Switzerland)
- Oxidation of wet biomass (UK)
- Modelling of biomass combustion (Norway)
- Co-firing of biomass and coal (UK)
- Combustion studies of pyrolysis oils and char (USA) [23]

Since this time, many different biomass technologies have been developed far beyond the conventional burner. Not only can biomass be used directly for energy, but it can also be converted into intermediate products to be utilised for energy generation or other uses. Some of the most important uses for biomass, other than direct combustion are:

- Gasification to produce syngas
- Liquefaction to produce liquid product
- Hydrolysis/Fermentation to produce bioethanol
- Transesterification to produce biodiesel
- Anaerobic digestion to produce biogas [15]

With regards to burner technology, one of the most important areas of study, currently, is *primary measures* for pollutant reduction. Primary measures include design optimisation of burners to create as low pollutant emissions as possible. This is one of the keys to making biomass combustion economically feasible, since post-combustion treatment of gases can greatly increase the capital cost of power plants. Studies of Austrian and Swiss furnaces have been used to empirically characterise the factors leading to NO_x production [36]. One of the most important factors affecting NO_x production is *air staging*, described in detail in section 2.2.2.

1.5 The pellet burner design in question

The following study is partly based on an existing biomass pellet burner design under development by *Departamento de Ingeniería Mecánica* at the *Universidad Politécnica de Madrid*[7]. Using this design as a base case, the operational parameters and design considerations will be analyzed using theory-based modeling. The goal will be to determine the best mix of design and operation settings for reducing pollutant emissions (especially NO_x and CO) while considering performance as well.

The burner design features four major chambers: the combustion chamber, the ash collection chamber, and the antechamber for each of these where primary and secondary air are fed. The main chambers are enveloped in an octagonal shape by carbon steel. In addition to the combustion chamber, there are air-bypass channels running around the chamber that prevent loss of heat to the ambient air. The pellets are fed into the combustion chamber via two feeding tubes coming from above and entering the chamber through the back wall. The pellets fed into the chamber fall onto a grate with three separate channels. These channels have slits to allow for

[7]Mechanical Engineering Department at the Polytechnic University of Madrid

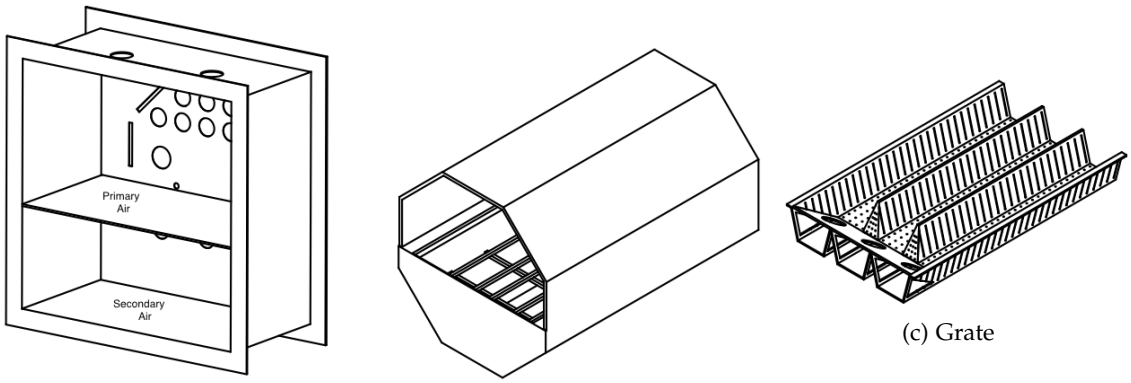

(a) Antechambers (b) Combustion Chambers (c) Grate

Figure 1.4: Prototype Design

the feeding of primary air. The pellets are moved through the combustion chamber using motorized screws: one for each channel.

The air is fed into the combustion chamber by two fans. A smaller fan feeds primary air into the lower antechamber. The air then flows into the main chamber entering from under the pile. A larger fan feeds secondary air into the upper antechamber and then into the combustion chamber. After the combustion chamber, the flue gas exits out the far end of the chamber for heat recovery.

The scale of the burner is intended for district heating for a community the size of an apartment complex. Various consultations were made in the field viewing pellet burners already in use in this context. The primary goal of their study is to develop prototypes to further investigate various design parameters of pellet burners. A prototype of the burner design was completed in July 2014 (see figure 1.5). The prototype was tested to ensure proper operation. New mechanical improvements are slated to be made, with experiments still ongoing. Emissions and thermal data are not yet available.

1.6 Motivation for including computational fluid dynamics

With the main focus of the design being the main design parameters and how they effect the burner performance, it is also important to supplement the prototypical approach with models that can provide further insight. In this thesis, the main goal will be to utilize fluid modeling in order to better understand how the burner design particularly affects the chemical processes occurring within the combustion chamber. To this end, it is important to know the dynamics of the fluids flowing through it, for this directly influences temperatures and mixing, and thus, reaction rates.

Computational fluid dynamics is a powerful tool that will allow estimating the velocity and temperature profiles within the combustion chamber. Furthermore, if there is not perfect mixing within the chamber, then it is clear that certain areas of the chamber will experience different reactions at different rates than others. Therefore, the design of the burner and how it influences these reaction regions and where they form is critical to understanding how the design affects the performance.

Figure 1.5: Burner Prototype

One particular application for this data is predicting how the design affects the production of pollutants. As stated before, pollutants formed by burning biomass present a new problem for biomass as an energy source. Also, before expensive post-treatment options are considered, it is important to first determine whether simple design parameters can be tweaked in order achieve a better outcome. If after all modifications, the pollutant production is still too high, post-treatment units can be used like SNCR, SCR, adsorbers, scrubbers, etc [25].

In the proceeding thesis report, the goal is to determine which design and operational parameters play the most important role in determining the production of pollutants.

Chapter 2

Theory

2.1 The full combustion process of biomass pellets

Combustion, in the strictest chemical sense, is the oxidation of all atomic species of a given compound. This means that every element present in a combustible fuel is transformed, via chemical reaction mechanisms, to its fully oxidized form. The most common examples of oxidized forms evolving from typical fuel species are as follows:

- $C + O_2 \rightarrow CO_2$
- $H + \frac{1}{4}O_2 \rightarrow \frac{1}{2}H_2O$
- $O \rightarrow \frac{1}{2}O_2$
- $S + \frac{3}{2}O_2 \rightarrow SO_3$
- $N + O_2 \rightarrow NO_2$

However, as chemical kinetics and thermodynamics dictate, combustion never takes place so simply and so completely. In every case, but in varying degrees, the burning of fuels also leads to the evolution of *partially* oxidized species such as CO, SO_2, and NO. The completeness of the combustion is a function of mainly the chemical composition of the fuel and the conditions under which the combustion is taking place (specifically the residence time and combustion temperature) [25]. Chemically-simple combustion fuels such as methane, the main component of natural gas, have a limited number of pathways through which they can be decomposed and then oxidized. Methane, the simplest hydrocarbon with the chemical formula CH_4, has four identical chemical bonds that must be broken in order to allow oxidation [2].

When it comes to the combustion of substances like the wood derivatives used in biomass pellets, the types of molecules in question could have potentially thousands

and thousands of chemical bonds to be broken. Many of these bonds are different in nature (meaning differences in bond energy, steric hindrance, etc.). With so many more complications, the simplistic combustion assumptions that would be considered for fuels such as methane utterly fail when it comes to describing complex molecules such as cellulose.

Another important consideration, reaching beyond the chemical perspective and entering the material property realm, is that the composition of the fuel is by no means homogeneous. Biomass, by virtue of its origins from living material, is highly compartmentalized into organized regions [52]. The organic mass of biomass is mainly composed of the following three types of chemical compounds:

- *Cellulose:* The primary component constituting the cell wall of plants. Cellulose provides the structure of the biomass and its presence is what normally allows biomass to retain its shape. Cellulose is a polysaccharide chain composed of glucose monosaccharides that have been joined together though dehydration synthesis[1] [52].
- *Hemicellulose:* Similar in composition to cellulose and also present in cell walls, hemicellulose can contain many different types of monosaccharides, and is therefore more branched and less uniform. Higher amounts of branching lead to less integrity and a more amorphous, less crystalline solid structure. Since this is true, the molecule is more exposed, leading to faster decomposition reactions.
- *Lignin:* Not composed of sugars, lignin is especially important to biomass because it makes the cells more rigid and has anti-rotting[2] properties [49].

The biomass can also contain other compounds, namely water, minerals, and lipids. Depending on the compositional makeup of the biomass, the mechanisms that it must take to reach complete combustion conditions vary greatly. According to a study by Ayhan Demirbas for Sulcuk University, cellulose and hemicellulose tend to volatilize while lignin tends to form solids [16]. All things considered, the typical biomass pellet combustion can usually be separated into three principal stages: water evaporation, pyrolysis, and char combustion. This separation is used by nearly every biomass model that has previously been developed [12, 41, 48].

2.1.1 Water evaporation

The first step in the typical combustion of a biomass pellet is drying. Since the moisture content of pellets makes up a fairly significant portion of their mass, the

[1] Dehydration Synthesis: The joining of two molecules at the point where each has a hydroxyl functional group. One molecule looses a hydroxide, the other looses a hydrogen, and the unpaired electrons resulting join the two molecules together forming a new covalent bond, releasing a free water molecule.

[2] Rotting is essentially the biological version of oxidation. Since the lignin prevents rotting of the plant, this means that the lignin, itself, will be oxidized.

evaporation properties associated with water become a bottlenecking step when it comes to heating up the pellet. Water, at atmospheric conditions, cannot reach temperatures above $100°C$. Any energy added to water at $100°C$ will go toward the latent heat of vaporization, and not toward sensible heat which would increase the temperature. So while water is still present within the biomass particle, it is difficult to heat it up beyond the boiling temperature of water. This becomes a limiting factor in the decomposition of the pellet, because pyrolysis of the major hydrocarbon constituents does not typically occur until temperatures reach above $300°C$ [34].

When considering the full process involved in the evaporation of a water molecule from inside of a biomass pellet into a vaporized form, it is necessary to consider the longest, most convoluted possible path that the molecule can take. Clearly, the water molecules in the center of the pellet have the longest path to travel. In order for a molecule to travel from the center of the biomass pellet to its final gaseous form, it must take the following steps:

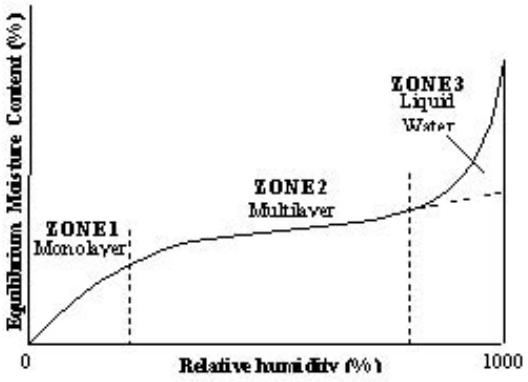

Figure 2.1: General shape of sorption isotherms [30]

1. *Migration to surface:* By means of either concentration-driven diffusion or capillary action due to H_2O's strong dipole moment, the water molecule must travel from the center of the pellet to the surface. This overall action can be summarized by an *effective diffusion coefficient*, D^{eff} [30].

2. *Equilibration at the surface:* In situations where an absorbed liquid is vaporizing, the driving force cannot simply be defined by the difference between the surface concentration and the vapor concentration. In the situation of wood sorption of water, the water at the surface forms a boundary layer several molecules thick. This phenomenon, thermodynamically speaking[3], is preferable since water molecules grouped together have lower energy due to hydrogen bonding. It becomes especially preferable for high concentrations of water at the surface. This equilibrium can be quantified using various empirical models. Therefore, water molecules must also reach a surface equilibrium concentration usually different from the concentration immediately within the pellet [11].

[3]The second law of thermodynamics implies that the change in Gibbs free energy of any spontaneous process must be negative, therefore the release of energy from a system to its surroundings is always thermodynamically preferable

3. *Convective mass transfer:* As stated in mass transport theory, the rate of convective mass transfer is proportional to a concentration-based driving force. In the case of wood drying, it is the difference in concentration of the equilibrated water at the surface with the steam in the vapor. In this process, the molecule must absorb enough energy from its surroundings to break the forces binding it to its neighbors and to vaporize, where it is virtually alone. This is the *latent heat of vaporization* [30].

It is also important to consider that, in order for the vaporization to take place, a sufficient amount of heat must be available in the surroundings. When considering the temperature profiles inside the pellet and around the pellet, it is essential to utilize the biot number, Bi.

$$Bi = \frac{h\ell}{k_p} \tag{2.1}$$

The biot number is a dimensionless ratio of the convective heat transfer rate with the conductive heat transfer rate. If Bi is significantly less than unity, then the temperature within the pellet can be considered to be uniform. The same consideration can also be made for the mass transfer profile, as expressed above. However, it will be shown that the Bi_m, or the mass biot number, is too high to consider the internal composition uniform.

2.1.2 Pyrolysis

After the particle has been voided of its moisture content, the temperature of the pellet can rise to temperatures sufficient for facilitating the pyrolysis reaction. Pyrolysis, by definition, is the thermal decomposition of larger molecules into smaller ones, in the relative absence of an oxidant [33]. A simple example of a pyrolysis reaction could be the following [27]:

$$CH_3CH_2CH_3 \xrightarrow{\Delta} \cdot CH_3 + \cdot CH_2CH_3$$

With increasing heat, particle collision frequency increases, inducing the tendency of molecules to break up into smaller molecules, including radicals, as shown above. Since the molecules in biomass are normally large, complex, and not uniform, predicting the potential pyrolysis products is incredibly difficult. Many complex reaction mechanisms have been proposed, often chosen to suit certain experimental conditions and very specific types of biomass fuel. One notable attempt at modeling the pyrolysis mechanism of cellulose is by Lin et al. at University of Massachusetts

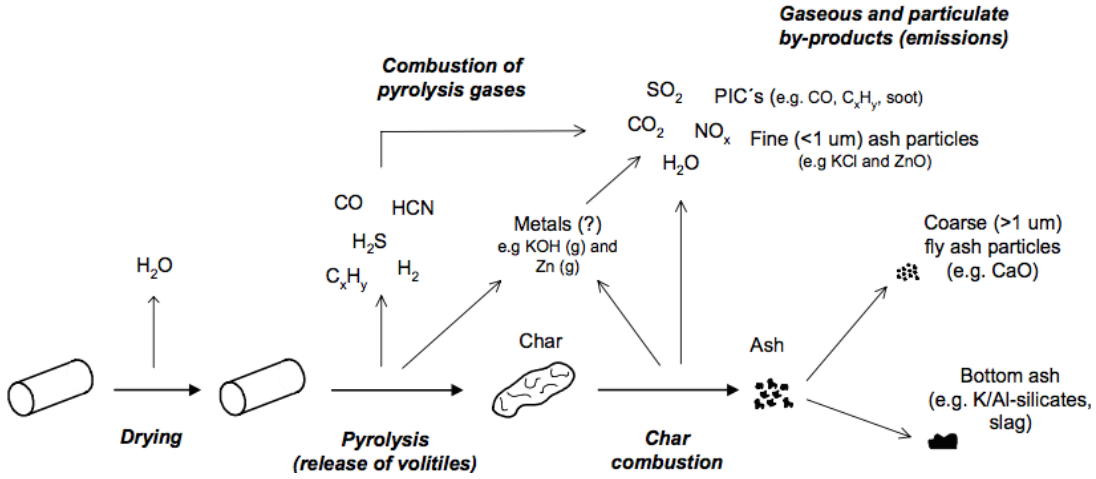

Figure 2.2: Different stages during combustion of a biomass fuel particle [13]

where they describe the formation of 14 different products. The model was verified using TGA-MS analysis[4] [28].

Pyrolysis also causes a physical change of the pellet itself. During pyrolysis reactions, the pellet will shrink by approximately one third of its volume [48]. In this process, large pores and cracks are formed when pockets of gaseous products trapped inside the pellets are released after accumulation of pressure. In this process, the excessive heats and air flow rates cause the blowoff of another material called *tar*. Tar consists of various large hydrocarbon molecules that are still large enough to remain in the liquid phase at moderate temperatures. Tar will either blow off or vaporize and then recondense in the vapor [15].

A simpler approach to model pyrolysis and the resulting gases is by combining empirical data with mass balances to account for the remainders. By considering the production of the easily quantifiable species, such as CO or H_2O, and considering the amount of char left, the remaining mass can be attributed to the presence of tar and other, harder-to-quantify, hydrocarbons in the pyrolysis gas [34].

2.1.3 Char combustion

After the pyrolysis of all available volatile material, what remains is *char*. This char is composed principally of carbon, and has similar properties to carbon-based solids such as graphite. The char also contains all of the ash content that was not blown off during the pyrolysis phase [34].

With most heteroatoms[5] gone after pyrolysis, the remaining carbon in the char begins to combust. The rate of this combustion can be highly dependent on the pore

[4]TGA-MS: Thermo-gravimetric Analysis - Mass Spectroscopy
[5]Heteroatoms, in this case, are H, O, N, and S

structure of the char (or the density) [38]. Biomass that is pyrolyzed quickly tends to have larger and deeper pores, while biomass that is pyrolyszed slowly will have narrower and less profound pores. The more pores that there are, and the deeper they go, the more access that oxygen has to the non-surface carbon in order to combust.

The kinetics of the char combustion are typically simpler than those of pyrolysis since the chemical composition of the fuel has been greatly simplified. The main considerations are the rate at which oxygen can diffuse to the surface of the char pellet, and the kinetics of the reaction itself once the oxygen has reached the surface. This rate is typically summarized using a first-order kinetic rate equation with respect to the partial pressure of oxygen in the gas [41].

As the char combusts, the pellet shrinks as layer after layer of carbon atoms are removed. Any remaining structure of the original pellet is lost completely during combustion. What remain afterward are minerals and metals in the form of ash with about 3% of the volume of the original pellet [48]. Depending on the temperature, this ash runs the risk of melting, resolidifying, and agglomerating. This is less of a problem in grate burners but more of a problem in fluidized beds and gasifiers [25].

2.2 Pellet burner design

As previously stated, the completeness of combustion directly depends on the composition of the fuel and the design of the burner where the combustion is taking place. When designing a pellet burner, the considerations must go beyond simply ensuring a complete combustion. In most developed countries, there are strict regulations limiting the amount of emitted pollutants allowed, many of which are potential products of pellet combustion, even when the fuel is completely oxidized. For example, in the Netherlands, there are specific emission limits for biomass pollutants like NO_x, dust, HX. and dioxins [25]. Depending on the final use of the energy, the design also needs to take into account whether or not the burner must be run in a *batch*[6] mode, *quasi-continuous*[7] mode, or a *continuous*[8] mode. A small scale residential burner would most likely be a batch process [23]. In a grate-stoker combuster, fuel can be fed intermittently, which would make it a quasi-continuous process [20]. While in larger-scale operations like gasifiers, continuous operation is key to maintaining high pressures [40].

[6]Batch: a chemical process where the reactants are charged once and then the reaction runs, with the status of the system varying over time

[7]Quasi-continuous: a chemical process that is fed reactant at certain time intervals; the system status varies with time periodically

[8]Continuous: the reactant is fed constantly into the system; the system does not change with time; synonymous with *steady state*

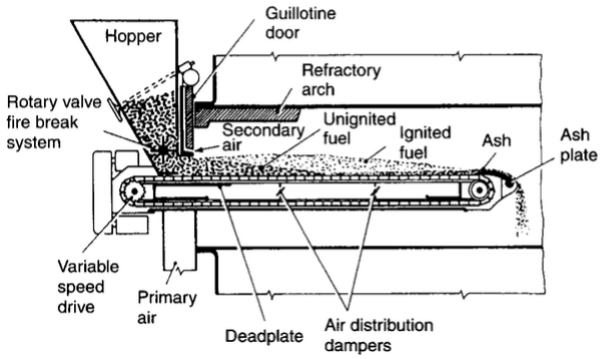

(a) Chain-grate stoker

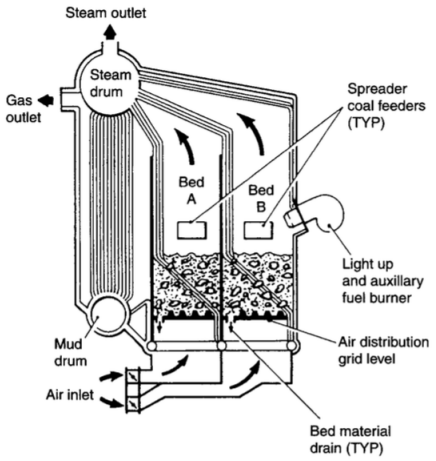

(b) Fluid-bed combustion system with sectioned bed

Figure 2.3: Burner configurations [17]

2.2.1 Grate burner configurations

Biomass burners, and solid fuel burners in general, have a wide range of designs which are still being developed today. Each of them has a series of pros and cons, and the choice of design is often completely dependent on the final use. On the smaller, residential-scale, big complicated systems requiring pressurized chambers and complex control systems are usually not economically feasible or mechanically efficient. It is much more common on this scale to gravitate toward a simple, fixed-grate burner configuration [23].

On larger, industrial or commercial scales, the economics of scale and the increasing mechanical efficiency with size, make more complex burners more feasible. One of the most important designs for research interest is the fluidized burner. In a fluidized burner, the biomass is usually suspended in a fluidized bed of mineral material (typically sand) that is kept suspended by high air velocities. In order to maintain such velocities through the bed, high pressure at the entrance of the combustion chamber is required. Since this design relies on the fluidity of the bed, it is vital that none of the resulting ashes sinter and clog the chamber. This means a complex heat rejection system also needs to be employed. While this design paradigm offers very interesting benefits with respect to pollutant control and higher boiler efficiencies, its lack of feasibility at small scales means it will not be of interest in this study [17].

Meanwhile, there are a variety of grate designs that attempt to mitigate the cons associated with the fixed design, while attempting to retain the major pro of low cost. Arguably, the most important function to be considered in grate design is the disposal efficiency of ash while retaining the fuel and allowing primary air[17]. The presence of ash after the last of the char is combusted is undesirable because it absorbs heat that could otherwise be utilized if it exited with the flue gas.

In order to facilitate this disposal and allow for a continuous feeding of fuel, one proposed grate modification has been the chain grate. The chain grate conveys the biomass through the combustion chamber, helping to mitigate the possible buildup of ash in certain places. In this study, the design in question involves a fixed grate with propulsory screws. The screws also help prevent stagnant ash buildup and agitate the fuel enough to allow an easier passage of air from underneath[17].

2.2.2 Primary air and secondary air

According to chemical stoichiometry, depending on the elemental composition of the fuel, there is a precise amount of oxidizer needed to perfectly oxidize the fuel, assuming that the reaction is able to go to completion. When the oxidizer is air, this amount divided by the amount of fuel is called the *air-fuel ratio.* It can be calculated using simple chemical equation balancing as shown:

$$C_{x'_C}H_{x'_H}O_{x'_O}N_{x'_N}S_{x'_S} + \left(x'_C + \frac{x'_H}{4} + x'_S - \frac{x'_O}{2}\right)O_2 \rightarrow x'_C CO_2 + \frac{x'_H}{2}H_2O + \frac{x'_N}{2}N_2 + x'_S SO_2$$

$$\alpha^{ST} \equiv \frac{m_{air}^{ST}}{m_F} = \frac{1 - Y_M - Y_a}{x_{O_2,0}} \frac{M_{air}}{M'_F}\left(x'_C + \frac{x'_H}{4} + x'_S - \frac{x'_O}{2}\right) \tag{2.2}$$

While in simple chemistry the stoichiometric amount of air is sufficient, in a complex situation such as a combustion burner involving two different phases of matter, considering stoichiometry alone seldom suffices. When the formation of CO, SO_2, and NO_x are so critical due to emission standards, the reaction, as shown already, must especially be discussed using more complex mechanisms. Since it is known that the combustion of the fuel does not take place in one simple step, it is possible that by controlling the feeding of the reactants, namely air, the stages of the combustion can be more carefully controlled.

By controlling the feeding of air into the burner chamber, it is possible to determine which stages of the combustion occur in which regions. The amount of air present determines whether or not the rate limiting step will be the pyrolysis or the combustion stage. It also determines how much NO_x is produced [57].

When considering the amount of air, it is often compared to the stoichiometric amount using the *equivalence ratio:*

$$\lambda = {}^{\frac{m_{air}}{m_F}}/_{\alpha^{ST}} \tag{2.3}$$

When λ is unity, this means that the amount of air fed is the stoichiometric amount. Depending on the equivalence ratio, the products expected from chemical reactions

vary greatly. Pyrolysis, by definition, is the thermal decomposition of molecules *without* the presence of oxygen [43]. Therefore, pyrolysis is generally favored when λ is low. With air levels much closer to unity, the products of the decomposition of fuel change. Decomposition under sub-stoichiometric air conditions is normally referred to as *gasification* . Typically the products of gasification are not in their more reduced forms as would be seen in pyrolysis. For instance, there are typically higher amounts of CO and H_2O and lower amounts of CH_4 and H_2 vis a vis the pyrolysis conditions *[53]*.

Since the pyrolysis reaction is less likely to produce NO_x than gasification or full combustion, it has become a commonplace technique, especially in nitrogen rich fuel burning such as biomass, to utilize what is called *air staging*. Air staging involves the injection of air in different areas of the combustion chamber at different rates [57]. In the hottest parts of the chamber, where the pellets are located, it is important to keep the oxidation relatively low, to prevent excessive NO_x production. So at the pellet bed, so-called *primary air* is injected at rates where λ is less than unity. With temperatures high and the O_2 concentration relatively low, this area forms a reduction zone that favors the reduced form of nitrogen, N_2, as opposed to the oxidized ones, NO_x [24].

In the areas downstream of the pellet pile, the temperature decreases rapidly. As the temperature decreases, the selectivity[9] of carbon and hydrogen oxidation increases with respect to nitrogen [18]. Therefore, it is optimal to inject an excess of air in this stage to favor as complete a combustion of carbon and hydrogen as possible. This second injection is called *secondary air* and it creates a combustion zone. Since the temperature is so much lower, the NO_x reaction kinetics dictate that hardly any more NO_x is formed in the combustion zone. It can be said that the NO_x composition is *frozen* at its concentration at the flame front [44].

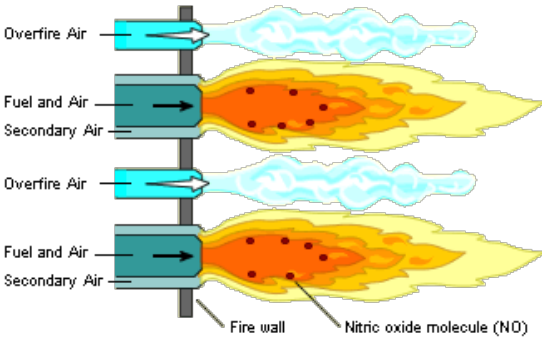

Figure 2.4: Air staging

Additionally, from a heat exchange standpoint, it is important to consider that too much excess air (secondary) will lower the temperature of the flue gas. If the flue gas temperature is too low, this would require designing an energy extracting steam cycle with much larger components. Therefore, it is important to consider both keeping the outlet concentration of undesired products low and making the flue gas temperature high enough for a feasible steam cycle [22].

[9]The ratio of the rate of production of desirable products over the undesirable products; higher selectivity does *not* imply faster kinetics.

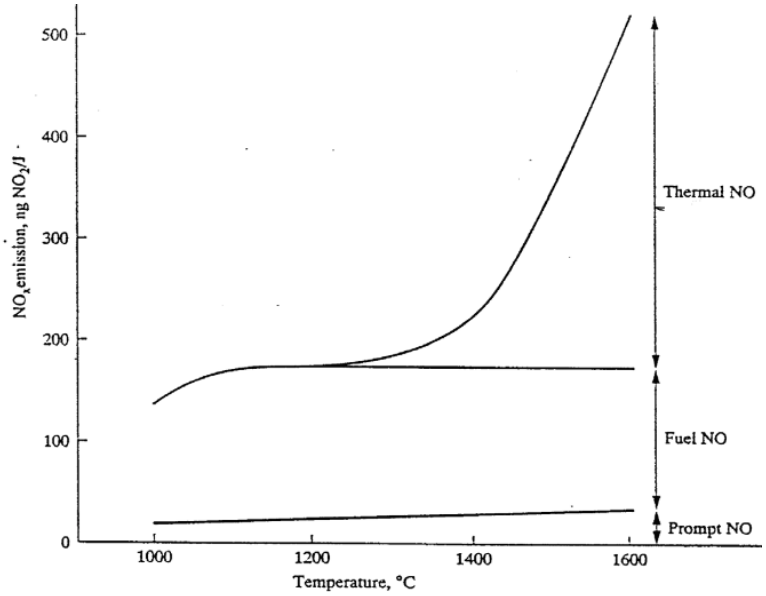

Figure 2.5: Contribution of different NO_x production mechanisms

2.3 Chemical considerations of pollutant production

2.3.1 *CO*

The production of carbon monoxide is inevitable in any combustion condition. According to nearly all proposed oxidation mechanisms of carbon, carbon monoxide is a precursor to carbon dioxide [9, 54]. However, the *combustion efficiency*[10], is highly dependent on how much oxygen is present and the residence time of the fuel and the gases in the combustion chamber. In the case of solid fuel, a large portion of the *CO* is generated during the pyrolysis phase when the fuel-bound oxygen partially oxidizes the fuel-bound carbon [34]. This *CO* then has the potential to be further combusted by the secondary air in the combustion zone[35]. The amount of this complete combustion is dependent on the combustion dynamics and will be discussed further in 2.4.2.

2.3.2 NO_x

The production of NO_x is an important consideration because it is a major cause of acid rain (via the reaction $NO_x + H_2O \rightarrow H_2NO_{x+1}$) and also a trigger of asthma in many people [13]. NO_x production is typically classified into three different mechanisms:

[10]Combustion Efficiency: the fraction of carbon that is fully oxidized; normally defined as $\frac{[CO_2]}{[CO]+[CO_2]}$

- Fuel NO_x: Nitrogen from the fuel has the potential to oxidize (NO_x) or reduce (N_2) depending on the amount of oxygen present during the pyrolysis stage. Since the amount binding energy between C and N is relatively low, Arrhenius-based kinetics dictate that the production has little to do with temperature.
- Thermal NO_x: Sufficient temperatures can cause scission in the $O = O$ bond of gaseous oxygen, releasing $O\cdot$ radicals with the potential of initiating a chain reaction with the gaseous nitrogen that can produce NO. The initiation step of this reaction is highly dependent on temperature, so this type of NO_x will only be formed at the hottest parts of the burner. Once exiting the hot areas, the reaction is said to be *frozen* at the exiting concentration. Since oxygen is part of the chain propagation steps, the concentration of oxygen is also key to the formation rates.
- Prompt NO_x: Similar to thermal NO_x, prompt NO_x is also triggered by radicals, but in this case by hydrocarbon radicals released as a result of pyrolysis. The amount of hydrocarbon radicals is not heavily dependent on temperature; however, since oxygen is again part of the chain propagation, the gaseous oxygen content does influence the production [54].

Each of these three mechanisms contribute to the overall NO_x production, with varying degrees depending on the O_2 concentration and the temperature.

2.3.3 SO_x / H_2S

SO_x production during the combustion of solid fuels is virtually unavoidable if there is sulfur present in the fuel [13]. The two options of mitigating SO_x in the flue gas are either pre-treating the fuel using chemicals like H_2O_2 or $FeCl_2(aq)$ (though this is not usually done for pelletized biomass) or post-treatment using adsorbers, scrubbers, or dry chemisorption. Any sulfur present in the fuel will more than likely be oxidized by the time the flue gas exits the burner. However, if the residence time or the oxygen content in the gas is low, then there is the potential that the reduced from, H_2S, could evolve. H_2S is initially formed during the pyrolysis step. Any remaining S in the solid char is oxidized and released as SO_x [33].

All things considered, since the sulfur content of pellet biomass is considerably lower than other solid fuels, especially fuel, sulfur emissions are not as significant as in other types of burners.

2.3.4 Volatile Organic Compounds

Volatile organic compounds, or VOCs, are any organic compounds that remain in a gaseous form at the final stack temperature. VOCs have detrimental health effects

ranging from acid rain to carcinogenic potential [13]. There are a great variety of chemical species that can compose VOCs including short-chain paraffins, low molecular weight aromatics, and organic acids. These species can potentially be generated during the pyrolysis step as well. Depending on the completeness of the combustion, there is the potential of releasing unburned hydrocarbons [54].

2.3.5 Fly Ash

The amount of ash released versus the amount retained is dependent on the grain size of the ash particles produced during the char combustion and the velocity of the primary air through the grate. If the drag is significant enough, the ash particles will become entrained in the gas flow and exit out the flue instead of going through the grate as intended [13]. The entrainment of fly ash can be related to particle size and air velocity by calculating the terminal velocity:

$$u_t = \frac{gd^2}{18\mu}\left(\rho_a - \rho_{air}\right) \tag{2.4}$$

If the terminal velocity is less than the velocity of the air, then the ash will be entrained.

2.4 Modeling of the temperature profile

When considering the temperature profile, it is important to consider the major generators, transmitters, and absorbers of heat. In this section, only the two most pertinent contributors to the heat will be discussed: the combustion of char and the combustion of the pyrolysis gases in the flame. These two reactions are exothermic and contribute the most to the temperature profile of the combustion chamber.

2.4.1 Char combustion considerations

At the point where all of the volatile material has evacuated what is left of the pellet, the resulting char will begin to combust [48]. This will typically be a slow burn due to the less-than-stoichiometric amount of oxygen fed from below in the primary air. When the combustion takes place, it is a reasonable assumption that this is a two-phase chemical reaction, and since the *volumetric* specific heat capacity of the air is so much higher than that of the char, it will be assumed that all of the thermal energy released in the combustion will be released at the surface of the char.

2.4.2 The flame formation and the *Eddy Break-Up Model*

Modeling the combustion of volatiles in the gaseous phase, essentially the flame itself, has proven to be a challenge for modern scientists and engineers. One of the most credible and widespread models being used for flames is the *Eddy Break-Up Model.* This model is often preferred due to its simplicity of modeling the combustion without the need of additional differential equations in the solving process. The Eddy Break-Up Model begins with one key assumption: the rate limiting step in the combustion is not the chemical reaction itself; it is the diffusion of the oxidizer to the fuel (or vice versa) [10].

Since the reaction kinetics no longer play a role in the rate, the reaction chemistry can be considered by the simple equation:

$$F + \nu_s O \rightarrow (1 + \nu_s) P$$

With this considered, all that matters as far as the chemical species goes is which of the species is limiting. This can be determined by stoichiometry. When this is included, the final rate with the inclusion of the diffusion considerations is as follows:

$$R_{comb} = C_{r1} \frac{\varepsilon}{k} \min \left[c_F, \frac{c_{O_2}}{\beta^{ST}}, C_{r2} \frac{c_P}{1 + \beta^{ST}} \right] \tag{2.5}$$

where C_{r1} and C_{r2} are model constants, and k and ε are system properties that will be described further in section 2.5.1 [10].

2.5 Solving mass, heat, and species transport equations

The partial differential equations arriving from the laws of conservation of momentum, energy, and mass are all parabolic, meaning they have the following form [39]:

$$d \frac{\partial \vec{u}}{\partial t} - \nabla \cdot (\mathbf{c} \otimes \nabla \vec{u}) + \mathbf{a} \vec{u} = \mathbf{f} \tag{2.6}$$

The significance of each variable and coefficient depend on the problem in question and whether the equation is employed as a momentum, energy, or mass balance. The specific forms of the equations will be discussed later.

Since all three conservation equations play a major role in the conditions within the burner, it is necessary to solve all three of them, simultaneously. Finding exact solutions of systems of PDEs is incredibly difficult. It reaches to the frontiers

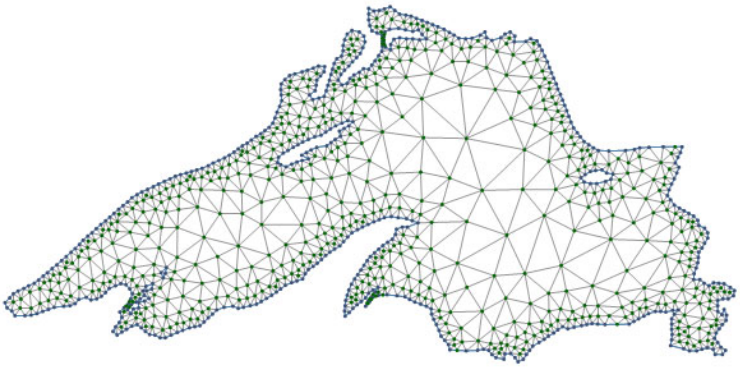

Figure 2.6: Meshing example of Lake Superior

of what mathematicians are able to calculate analytically. Therefore, it is reasonable, within a certain degree of accuracy, to resort to approximate solution methods for solving the system. Several software packages exist that are capable of solving computational fluid dynamics problems including ANSYS Fluent and COMSOL Multiphysics. These programs rely on meshing algorithms that take solid geometric objects and turn them into a discrete set of points, thus turning the system of PDEs into a larger but simpler system of ODEs. This approach is known as the *finite element method*.

The subsequent solving of the ODE system can be done using approximation methods such as the Galerkin method of weighted residuals or the boundary element method. The choice depends on the stiffness of the problem and other properties of the geometry over which to solve the system [39].

2.5.1 Computational Fluid Dynamics

Solving the momentum transport problem, via computational fluid dynamics (CFD), proves to be the most difficult of the three, due to the unique complication of turbulence. The forms of the momentum conservation PDE that represent velocity, $\vec{u}$, as only the superficial value, such as the Cauchy Momentum equation or the Navier-Stokes, do not take into account the fluctuations, or the deviations from the superficial average, due to turbulence [50]. This neglect is acceptable when considering low-velocity problems where the flow is laminar only, but when considering problems with the Reynolds number on the order of 10^4 or more, the implication does not suffice[11] [50].

In order to account for the turbulent fluctuation, a new dependent variable must be defined and inserted into the momentum equations:

[11] Reynolds Number: $Re \equiv \frac{\rho u d}{\mu}$; $Re < 2300$ laminar flow; $2300 \leq Re < 10000$ transitional flow; $Re \geq 10000$ turbulent flow

$$\vec{u} = \vec{U} + \vec{u'} \tag{2.7}$$

When inserted into the Navier-Stokes equations, this approach is known as Reynolds Averaged Navier-Stokes (RANS). The original velocity term is now split into the mean portion, $\vec{U}$, and the fluctuation portion, $\vec{u'}$. When plugging this back into the PDE, the terms corresponding to $\vec{U}$ are the normal terms that would be expected as before. The new terms that arise due to the inclusion of $\vec{u'}$ add the effects of turbulent fluctuations, and these effects must be somehow modeled [50].

One of the most common methods, and the one used in this study, is called the k-ε method. k is the turbulent kinetic energy and ε is the dissipation. Separate PDEs for these equations are solved simultaneously with the momentum, yielding the fluctuation term in the momentum PDE and the full effect of turbulence captured in the momentum balance [50]. These topics are explained in far greater detail in Applied Mathematics and Modeling for Chemical Engineers by Richard Rice and Duong Do [39].

Chapter 3

Method

The methodology for modeling the combustion of pellets will be separated into three principle levels: the single-pellet scale, the pellet pile scale, and the entire burner scale. Considering all three scales simultaneously would be a near herculean task both conceptually and computationally. Therefore, each of these will be considered quasi-independently, by making several key, educated assumptions that will allow starting at the pellet level and eventually considering the entire burner as a whole.

For the parameterization of the model, the composition of the inlet pellets will be considered fixed. This assumption means that only one type of pellet is used. Though this is not indicative of typical operation, since this study has the main goal of characterizing the effects of *operating and design conditions* on pollutant formation, the varied parameters will be the operating parameters and the burner design only.

3.1 Modeling of the pellets

As previously stated, the first modeling efforts will be made on the single-pellet level. It will be assumed that each of the three major steps of the combustion of the pellets takes place sequentially and basically begins immediately after the termination of the previous step. This is a common assumption made in many pelletized biomass combustion models. The most common convention is to consider the evolution of the biomass to follow four basic types:

- *Wet:* The wet pellets give off water vapor through evaporation. The heat required to evaporate the water does not reach all the wet pellets at once, so the wet pellets furthest away from the flame heat do not emit water vapor. In order to evaporate the water, heat is absorbed from the gas.
- *Dry:* Dry pellets are considered to have 90% of the original volume due to de-swelling. They contain all of the original pellet matter except the moisture. They undergo pyrolysis and give off devolatilized species, and in the process absorb heat.

Figure 3.1: Steps of pellet combustion

- *Char:* After autoignition due to high temperatures, the char pellets undergo combustion and emit CO_2 as a result. The composition is any carbon not volatilized and the ash content. They have 65% of the original pellet volume. In the combustion process, they release heat. Also, since they are on the top layer of the pile (see 3.2.1), the char pellets emit radiation heat (net effect) to the environment.
- *Ash:* The ash content constitutes 3% of the original pellet volume. The ash is chemically inert but does have the potential to absorb heat or fly out the flue Thunman and Leckner [48].

The pellets will be assumed to be perfect cylinders. In order to evaluate the biot number of a cylinder, as discussed previously, the characteristic length must be calculated as follows:

$$\ell = {}^{V}/_{A_s} = \frac{1}{{}^{4}/_{d} + {}^{2}/_{L}} = \frac{1}{{}^{4}/_{6mm} + {}^{2}/_{25mm}} \approx 1.34mm \tag{3.1}$$

3.1.1 One-particle model of evaporation

The water transport within the pellet will be modeled using the conservation of mass formula as follows Deen [14]:

$$\frac{\partial c_M}{\partial t} = D^{eff} \nabla^2 c_M \tag{3.2}$$

As previously stated, the diffusion and capillary motion within the pellet are lumped into one parameter, D^{eff}. When considering the conservation of mass equation above, the following assumptions (beyond the conservation of mass) have been made:

- There is no convective flow of water within the pellet[1].

[1]Typically the term, $\nabla \cdot (\vec{u} c_M)$, is included on the lefthand side of the equation to consider internal convection.

- Fick's first law, $\vec{j}_M = -D^{eff}\nabla c_M$, is an accurate representation of the driving force behind water flux.
- D^{eff} is constant with respect to temperature and position.

The initial condition of the PDE is defined as the initial moisture content of the pellet, c_{M0}:

$$c_M\left(t = 0, \forall\left\{r, z\right\}\right) = c_{M0} \tag{3.3}$$

assuming that the moisture content is initially uniform.

The boundary conditions of the pellet are a bit more complicated. Since there is a boundary layer of water at the surface, the mass flux at the boundary is driven by the difference between the air partial pressure of water and the equilibrium vapor pressure of the boundary layer, as follows:

$$\left.\frac{\partial c_M}{\partial r}\right|_{\forall t, r=\frac{d}{2}, \forall z} = -k_M\left(p_M^* - p_{H_2O}\right) \tag{3.4}$$

$$\left.\frac{\partial c_M}{\partial z}\right|_{\forall t, \forall r, z=0 \vee L} = -k_M\left(p_M^* - p_{H_2O}\right) \tag{3.5}$$

Calculation of the boundary layer equilibrium vapor pressure, p_M^*, is done using empirical models created using existing data. Several older models such as Hailwood and Horrobin are based off of a semi-empirical approach that begins with theoretical assumptions (such as how many molecules thick the boundary layer is), while newer models, which have better agreement with experimental data, take a purely empirical approach [11]. The model used in this study is the Malmquist model (parameters in algorithm 3.1), defined as follows:

$$p_M^* = \frac{p_{H_2O}^*}{1 + \left\langle \frac{1}{n}\left\{\frac{m_s}{M_{H_2O}}\left[\left(1-\theta_p\right)\frac{\rho_{H_2O}}{c_{M0}} + \theta_p\frac{\rho_p}{c_M}\right] - 1\right\}\right\rangle^{3/i}} \tag{3.6}$$

Since the surface temperature appears to play a significant role in the equilibrium behavior of the boundary layer, the energy balance equation within the pellet will also be solved as follows [14]:

$$\frac{\partial}{\partial t}\left(\rho c_p T\right) = \nabla\cdot\left(k_p \nabla T\right) \tag{3.11}$$

In order to formulate the energy balance in this form, the following assumptions have been made:

Algorithm 3.1 Malmquist Model Functional Parameters [3, 11]

$$\log_{10} p^*_{H_2O} = A - \frac{B}{T + C} \tag{3.7}$$

$$m_s = -5.8954 \cdot 10^{-7} T^2 - 9.736 \cdot 10^{-5} T + 0.40221 \tag{3.8}$$

$$n = -2.1825 \cdot 10^{-6} T^2 + 0.018552 T - 2.6939 \tag{3.9}$$

$$i = 2.0637 \cdot 10^{-6} T^2 - 0.0016742 T + 2.2885 \tag{3.10}$$

- There is no convective flow within the pellet.
- Fourier's Law, $\vec{q}'' = -k_p \nabla T$, is an accurate representation of the driving force causing conductive heat flux within the pellet.

The major difference between the heat balance equation and the mass balance equation is that the coefficients used in the heat balance equation are not necessarily constant. The density, the specific heat capacity, and the conductivity all depend on the water content, c_M, which is a function of both position and time. Therefore, these coefficients cannot be pulled outside of the differential operators and must be conserved when solving the PDE. To calculate the values of each of these properties, a weighted approach is used [26, 30]:

$$X = X_M Y_M + X_p \left(1 - Y_M\right) \tag{3.12}$$

3.1.2 The pyrolysis and combustion of the pellets

In the case of pyrolysis and the combustion of pellets, internal diffusion rates and equilibration at the surface condition do not have an effect in the considerations. The water has this effect because it remains liquid within the solid structure. The dry pellet remaining after the evaporation has no liquid components and therefore diffusion of species to the surface does not apply. Also, the conduction effects of heat can be shown to be negligible by evaluating the biot number:

$$Bi = \frac{h\ell}{k_p} \approx 0.215 \tag{3.13}$$

Since the internal profile of the pellet is considered to be uniform, the pyrolysis and combustion can be modeled using simple ODE's without considering spacial dimensions. The pyrolysis of the pellet can be expressed using the following equation [41]:

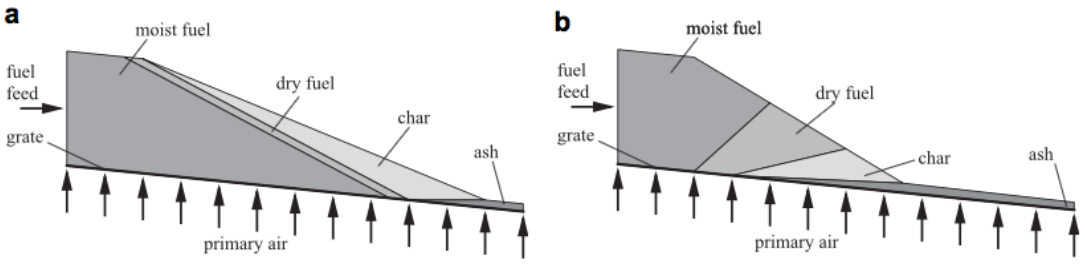

Figure 3.2: Countercurrent (a) and co-current (b) heat propagation profiles

$$\frac{d\rho_p}{dt} = -k_v \exp\left[-\frac{E_v}{R_{IG}T_p}\right](\rho_p - \rho_f) \tag{3.14}$$

Since the char combustion contributes to most of the pellet shrinkage, the extent of the combustion reaction can be related to the radius of the pellet. When substituting the diameter into the kinetic equation, the char combustion equation becomes [41]:

$$\rho_p \frac{d}{dt}(d) = -k_c \exp\left[-\frac{E_c}{R_{IG}T_p}\right] x_{O_2}^n \tag{3.15}$$

3.2 Considering the profile of the pellet pile

The burner design considered in this report is based on a previously developed design from the *Departamento de Ingeniería Mecánica* at the *Universidad Politécnica de Madrid*[2]. In this design, the biomass is fed onto a horizontal grate with three channels. Each channel has a rotating screw which propels the pellet pile forward, allowing for a continuous or quasi-continuous[3] pellet feeding. For the pile conditions along the direction of flow, it will be assumed that the material system is closed in the parallel direction. This means that the flow of mass in the horizontal is dependent only on the propulsion of the pellets and not by diffusive or convective mechanisms. Considering the pile in this manner, the pile system (in 2-D) has two independent variables: the vertical coordinate and time.

As the pellets enter in a uniform composition, the first layer of pellets begin to dry, and then pyrolyze. These steps are facilitated by manual heat injection (in the startup of the burner) or by heat generated by the char combustion. Once the dry pellets have lost all of their volatile material, they begin to combust and release heat. Depending on which direction this heat flows, the pellet profile can take different forms.

The equations and methods described in this section will be incorporated into a MATLAB model. The code for this model is included in appendix A.

[2]Mechanical Engineering Department at the Polytechnic University of Madrid

[3]Semi-continuous pellet feed was utilized in the first experiments of the prototype before the screws were working.

3.2.1 Co-current versus countercurrent heat propagation

In the modeling of pellet piles in one spacial dimension, there are two different phenomena that have been proposed: the co-current and the countercurrent heat propagation.

- *Co-current:* In the co-current case the heat travels in the same direction as the primary air flow. This implies that the ignition of the pellets occurs at the bottom of the pile. Some have suggested that the ignition occurs due to the conduction of heat in the grate itself. If this is true, then a layer of char will form at the bottom of the pile, and the heat from its combustion will dry and pyrolyze the pellets above it. This scheme is far less utilized in biomass combustion models, and it has been shown that it would best apply in cases of very moist fuel ($w_m > 50\%$).
- *Countercurrent:* The countercurrent model suggests that instead of being ignited at the bottom, the pile is ignited at the top and the heat flows against the air flow, via conduction through the pellet pile. In this case, the char layer forms on the top. The heat then flows down to allow drying and pyrolysis [48].

In this study, the countercurrent heat flow is assumed because of observed operations of the burner in experiments. This is supported by numerous other modeling studies of grate burners [26, 42, 51]. The flame front, under steady operation, developed across the majority of the pile, as supported by countercurrent, instead of at the end of the pile as supported by co-current.

3.2.2 Using the evaporation profile and the pile data to find overall evaporation rate

For a complete model, the pile calculus would need to be solved at the same time as the gas in order to describe the system in full. However, if certain assumptions are made and a set pile profile is assumed, then for the evaporation, pyrolysis, and char combustion, simple mass balances and kinetic equations are all that are needed to calculate the rates.

For the wet pellet section of the profile, it will be assumed that there are two regions: the evaporation region and the inert region. This approach borrows from the modeling of adsorbers as a mass transfer zone and a saturated zone [37]. The adsorption process is essentially the reverse of the drying process.

Since the heat of the char combustion will only reach so deep in the pile, only an upper portion of the wet pellets will evaporate at a given time. Within the section of pellets evaporating, the profile of evaporation rate versus time, calculated on a single

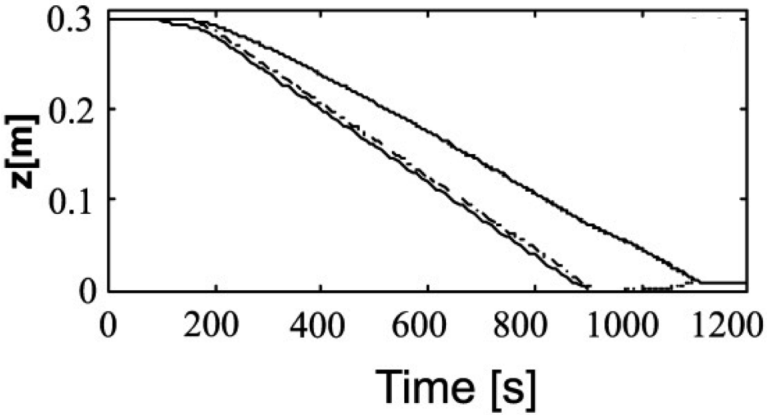

Figure 3.3: Pile profile used in model [48]

particle basis in 3.1.1, can be superimposed and transformed from time to a vertical, spacial basis. By either account, the average water concentration within a pellet in the midst of drying can be calculated as a time and volume average:

$$\bar{c}_{MZ} = \frac{1-\phi}{V t_{ev2}} \int_0^{t_{ev2}} \left(\oint_V c_M dV \right) dt \tag{3.16}$$

For simplification purposes, it will be assumed that the entire evaporating zone has the averaged moisture concentration [37].

The geometry of the wet zone of pellets is characterized by a flat section, where the wet pellet count doesn't change, followed by a section with a constant slope. In order to characterize the total shape, three parameters are needed: the initial height of the pile, h_0, the time when the wet section begins to shrink, t_{ev1}, and the time when the wet pile disappears, t_{ev2}. If it is assumed that the evaporation zone has a constant length (when fully developed) and a constant velocity in the downward direction, then these three parameters can be used to calculate this length and velocity:

$$u_Z = \frac{h_0}{t_{ev2} - t_{ev1}} \tag{3.17}$$

$$\bar{L}_Z = v_Z t_{ev1} \tag{3.18}$$

If the length and speed of the evaporation zone is known, then the evaporation zone length can be calculated as a function of time. It will be constant when it is fully developed, but at the beginning and the end of the pile, it will be smaller:

$$L_Z(t) = \begin{cases} u_Z t & t \leq t_{ev1} \\ \bar{L}_Z & t < t \leq t_{ev2} - t_{ev1} \\ u_Z (t_{ev2} - t) & t_{ev2} - t_{ev1} < t \leq t_{ev2} \\ 0 & t_{ev2} > 0 \end{cases} \tag{3.19}$$

Then the length of the inert section can also be calculated:

$$L_I(t) = \begin{cases} h_0 - u_Z t & t \leq t_{ev2} - t_{ev1} \\ 0 & t > t_{ev2} - t_{ev1} \end{cases} \tag{3.20}$$

Using these two lengths and the concentrations in the reaction zone and the inert zone, the total mass of moisture in a vertical differential cross section can be mathematically represented. Using this mass then differentiating, the total evaporation rate can be evaluated as a function of time:

$$m_M = A_x \left[L_Z \bar{c}_{MZ} + L_I c_{M0} \right] \tag{3.21}$$

$$R_{ev}(t) = -\frac{1}{A_x \bar{L}_Z} \frac{dm_M}{dt} = -\frac{1}{\bar{L}_Z} \left[\bar{c}_{MZ} \frac{dL_Z}{dt} + c_{M0} \frac{dL_I}{dt} \right] \tag{3.22}$$

3.2.3 Calculating the pyrolysis rate

The pyrolysis rate, as stated in 3.1.2, is directly proportional to the amount of volatilizable material present. In addition, judging by the typical profile, the rate at which pyrolyzable material becomes available after the drying quickly reaches equilibrium with the pyrolysis rate, because the thickness of the dry section remains mostly constant.

If it is assumed that the amount of pyrolyzable material present is directly proportional to the height of the dry section (meaning that the composition of volatiles within the pellets in the dry section will be approximated to be constant [37]), then instead of a mass balance of the pyrolyzable material, a "height balance" can be utilized. This will take into account the "inlet height" (first term on the right hand side in equation 3.23) resulting from wet pellets drying" and the "outlet height" (second term on the right hand side in equation 3.23) which is directly related to the pyrolysis rate. The height balance, in differential form should look like this:

$$\frac{dh_d}{dt} = \dot{h}_{in,d}(t) - k_v h_d \tag{3.23}$$

The "inlet" is simply the negative rate of change of the height of the wet section (inert and evaporation zones):

$$\dot{h}_{in,d}(t) = -\frac{d}{dt} \left[L_Z(t) + L_I(t) \right] \tag{3.24}$$

The value of k_v can be evaluated using the given profile if the steady state dry height is known. Observing the pile profile, it is clear that the steady state condition occurs between t_{ev1} and t_{ev2}. So the steady state condition will be evaluated at this interval:

$$\dot{h}_{in,d}(t_{ev1} < t < t_{ev2}) = -\frac{dL_Z}{dt} - \frac{dL_I}{dt} = u_Z \tag{3.25}$$

$$\frac{dh_d}{dt} = 0 = u_Z - k_v h_d^{SS} \tag{3.26}$$

$$k_v = \frac{u_Z}{h_d^{SS}} \tag{3.27}$$

Using the "outlet height," if the concentration of the pyrolyzable material in the dry section is defined, then the pyrolysis rate can be defined as follows:

$$\frac{dm_v}{dt} = -k_v h_d A_x \bar{c}_v \tag{3.28}$$

$$R_v = -\frac{1}{A_x h_d}\frac{dm_v}{dt} = k_v \bar{c}_v \tag{3.29}$$

3.2.4 Calculating the combustion rate of char

In the combustion rate calculations, many of the assumptions will be the same as those made for the pyrolysis. The height will be considered to be directly proportional to the combustable fuel available, meaning that the concentration of C will be considered constant in the char region. The combustion rate, however, is not proportional to the amount of C present, only to temperature and oxygen concentration in the air, as shown by equation 3.15. So with respect to the calculations at hand, the combustion rate will be considered constant.

The same type of "height balance" will be used for the char:

$$\frac{dh_c}{dt} = \dot{h}_{in,c}(t) - \dot{h}_{comb} \tag{3.30}$$

$$\dot{h}_{in,c}(t) = k_v h_d(t) - \dot{h}_{in,d}(t) \tag{3.31}$$

In order to evaluate the value of $\dot{h}_{comb}$ using the pile profile, the curve can be fit to one known height, for example, the height of the char section at t_{ev2}. The height

of the char at this point is approximately the whole height of the pile. Using these values, the needed value can be solved for as follows:

$$h_c\left(t_{ev2}\right) = \int_{t_{ev1}}^{t_{ev2}} \frac{dh_c}{dt} dt = \int_{t_{ev1}}^{t_{ev2}} \left[\dot{h}_{in,c}(t) - \dot{h}_{comb}\right] dt = \int_{t_{ev1}}^{t_{ev2}} \dot{h}_{in,c}(t) dt - \int_{t_{ev1}}^{t_{ev2}} \dot{h}_{comb} dt \tag{3.32}$$

$$\dot{h}_{comb} = \frac{\int_{t_{ev1}}^{t_{ev2}} \dot{h}_{in,c}(t) dt - h_c\left(t_{ev2}\right)}{t_{ev2} - t_{ev1}} \tag{3.33}$$

With this, the same approach can be used to calculate the char combustion rate. The only major difference: in order to avoid a divide by zero situation, the average char height is used instead of the instantaneous one:

$$\frac{dm_c}{dt} = -\dot{h}_{comb} A_x \bar{c}_c \tag{3.34}$$

$$R_c = -\frac{1}{A_x \bar{h}_c} \frac{dm_c}{dt} = \frac{\dot{h}_{comb} \bar{c}_c}{\bar{h}_c} \tag{3.35}$$

3.2.5 Considering the difference between fly ash and bottom ash

For the ash, it is assumed that any ash that is not depicted in the pellet profile has gone out with the flue gas as fly ash . First, disregarding the profile of ash in the bed, the amount of ash produced, by height, can be calculated as follows:

$$\frac{dh_a}{dt} = \dot{h}_{in,a}(t) \tag{3.36}$$

$$\dot{h}_{in,a}(t) = \dot{h}_{comb} - \dot{h}_{in,c}(t) \tag{3.37}$$

Once the total ash height[4], h_a, is evaluated, it can then be compared with the pellet profile to see how much has remained and how much has flown away. To characterize the profile of the bottom ash, two additional parameters can be used: the final bottom ash height, h_{ba}^{SS}, and the time when it reaches that height, t_{ba}^{SS}. Then, the height balance can be simulated using the profile:

[4]The total ash height is a virtual combination of the bottom ash height and the fly ash height if it would not fly off.

$$h_{ba}(t) = \begin{cases} 0 & t < t_{ev2} \\ h_{ba}^{SS} \frac{t - t_{ev2}}{t_{ba}^{SS} - t_{ev2}} & t_{ev2} \leq t < t_{baf} \\ h_{ba}^{SS} & t \geq t_{ev2} \end{cases} \tag{3.38}$$

With the quantity of bottom ash known, any remaining ash becomes fly ash. This can be evaluated using a method similar to the reaction rates in previous sections. However, this rate will be described as a flux since the ash evolves from the surface of the pile and not a region:

$$\frac{dh_{fa}}{dt} = \frac{dh_a}{dt} - \frac{dh_{ba}}{dt} = \dot{h}_{in,a}(t) - \frac{dh_{ba}}{dt} \tag{3.39}$$

$$\frac{dm_{fa}}{dt} = c_a A_x \frac{dh_{fa}}{dt} \tag{3.40}$$

$$J_{fa}(t) = \frac{1}{A_x} \frac{dm_{fa}}{dt} = c_a \frac{dh_{fa}}{dt} \tag{3.41}$$

3.3 Computational Fluid Dynamics

For the conditions in which the entire burner will be modeled, it has been determined that the most pertinent condition is in the condition of steady state operation. The solving methods would be different if the burner conditions were modeled during startup or shutdown. While these conditions are significant in terms of operational efficiency, for example the amount of time that it takes to reach steady state operations, they do not constitute the majority of operation time, with respect to the burner design in question [23]. Therefore, the focus of this study will be steady state; and therefore, the derivative of any variable with respect to time ($\frac{\partial}{\partial t}$) will be zero.

In order to translate the 1-D pile calculations into two dimensions, the time coordinate is transformed into a spacial coordinate by simply using the horizontal pile velocity, u_p:

$$x \equiv u_p t \tag{3.42}$$

Algorithm 3.2 RANS Model with k-ε [4]

$$\nabla \cdot (\rho \vec{u}) = 0 \tag{3.43}$$

$$\begin{aligned} &\rho \left(\vec{u} \cdot \nabla\right) \vec{u} = \\ &\nabla \cdot \left[-p\mathbf{I} + (\mu + \mu_T)\left(\nabla \vec{u} + (\nabla \vec{u})^T\right) - \tfrac{2}{3}(\mu + \mu_T)(\nabla \cdot \vec{u})\,\mathbf{I} - \tfrac{2}{3}\rho k \mathbf{I}\right] \end{aligned} \tag{3.44}$$

$$\rho \left(\vec{u} \cdot \nabla\right) k = \nabla \cdot \left[\left(\mu + \frac{\mu_T}{\sigma_k}\right) \nabla k\right] + P_k - \rho \varepsilon \tag{3.45}$$

$$\rho \left(\vec{u} \cdot \nabla\right) \varepsilon = \nabla \cdot \left[\left(\mu + \frac{\mu_T}{\sigma_k}\right) \nabla \varepsilon\right] + c_{\varepsilon 1} \frac{\varepsilon}{k} P_k - c_{\varepsilon 2} \rho \frac{\varepsilon^2}{k} \tag{3.46}$$

$$\mu_T = \rho C_\mu \frac{k^2}{\varepsilon} \tag{3.47}$$

$$P_k = \mu_T \left[\nabla \vec{u} : \left(\nabla \vec{u} + (\nabla \vec{u})^T\right) - \frac{2}{3}(\nabla \cdot \vec{u})^2\right] - \frac{2}{3}\rho k \nabla \cdot \vec{u} \tag{3.48}$$

3.3.1 Modeling the momentum transport of the gases

Using the RANS model with the k-ε method, the resulting momentum transport equations are displayed in algorithm 3.2.

These equations are defined within the entire burner volume. They must be solved simultaneously. At the inlet conditions, the boundary values are defined as follows:

$$\vec{u} = -U_0 \vec{n} \tag{3.49}$$

$$k = \frac{3}{2}\left(U_0 I_T\right)^2 \tag{3.50}$$

$$\varepsilon = C_\mu^{3/4} \frac{k^{3/2}}{L_T} \tag{3.51}$$

At the outlet conditions, the boundary values are defined as follows:

$$\left[-p\mathbf{I} + (\mu + \mu_T)\left(\nabla \vec{u} + (\nabla \vec{u})^T\right) - \frac{2}{3}(\mu + \mu_T)(\nabla \cdot \vec{u})\,\mathbf{I} - \frac{2}{3}\rho k \mathbf{I}\right] \vec{n} = -p_0 \vec{n} \tag{3.52}$$

$$\nabla k \cdot \vec{n} = 0 \tag{3.53}$$

Algorithm 3.3 Mass Transport of Concentrated Species [4]

$$\nabla \cdot \vec{j_i} + \rho \left(\vec{u} \cdot \nabla \right) Y_i = R_i \tag{3.60}$$

$$\vec{j_i} = - \left[\rho \left(D_i^m + \frac{\nu_T}{Sc_T} \right) \nabla Y_i + \rho Y_i D_i^m \frac{\nabla \bar{M}}{\bar{M}} + D_i^T \frac{\nabla T}{T} \right] \tag{3.61}$$

$$D_i^m = \frac{1 - Y_i}{\sum_{k \neq i} {}^{x_k}/_{D_{ik}}} \tag{3.62}$$

$$\bar{M} = \left[\sum_i {}^{Y_i}/_{M_i} \right]^{-1} \tag{3.63}$$

$$\nabla \varepsilon \cdot \vec{n} = 0 \tag{3.54}$$

At the walls, the boundary conditions are defined as follows:

$$\vec{u} \cdot \vec{n} = u_s \tag{3.55}$$

$$\left[\left(\mu + \mu_T \right) \left(\nabla \vec{u} + \left(\nabla \vec{u} \right)^T \right) - \frac{2}{3} \left(\mu + \mu_T \right) \left(\nabla \cdot \vec{u} \right) \mathbf{I} - \frac{2}{3} \rho k \mathbf{I} \right] \vec{n} = -\rho \frac{u_\tau}{\delta_w^+} \vec{u}_{tan} \tag{3.56}$$

$$\vec{u}_{tan} = \vec{u} - \left(\vec{u} \cdot \vec{n} \right) \vec{n} \tag{3.57}$$

$$\nabla k \cdot \vec{n} = 0 \tag{3.58}$$

$$\varepsilon = \rho \frac{C_\mu k^2}{\kappa_v \delta_w^+ \mu} \tag{3.59}$$

3.3.2 Modeling the mass transport of the concentrated gaseous species

In the calculations, the gaseous species are separated into 5 major components: N_2, O_2, CO_2, H_2O, and pyrolysis gases (as a lumped species, see section 3.3.3). Any other gases will be considered to be dilute enough that they do not contribute to the overall molar volume. The mass transport equations are defined as follows:

At the walls, the boundary condition is:

$$\vec{n} \cdot \left(\vec{j_i} + \rho \vec{u} Y_i \right) = 0 \tag{3.64}$$

At the outlet, the boundary condition is:

$$\vec{n} \cdot \rho D_i^m \nabla Y_i = 0 \tag{3.65}$$

At the inlets, the boundary condition is:

$$Y_i = Y_{i0} \tag{3.66}$$

In order to consider the species introduced into the gas by the reactions, the regions of the pile where the reactions occur are clearly defined in the geometry: the wet evaporation zone, the dry zone, and the char zone. In the wet evaporation zone, the reaction rate is defined as stated in equation 3.22, using the time to space transform in equation 3.42. The pyrolysis and combustion rates in the dry and char zones come from equations 3.29 and 3.35, respectively.

3.3.3 Modeling the gaseous combustion of pyrolysis gases

3.3.3.1 Pyrolysis Product Model

After the pyrolysis products enter the gaseous phase, they must be considered as viable candidates for gaseous combustion. Depending on the composition of the pyrolysis products, the combustion stoichiometry and LHV can vary. In order to calculate the composition of the pyrolysis gas, an empirical mass balance approach is borrowed from Neves et al. In their method, they use collected data to model the product production as a function of the biomass ultimate analysis data and the pyrolysis temperature. The remaining unknowns are calculated using mass and energy balances. The resulting system for calculating the pyrolysis gases is presented below [34]:

$$\begin{bmatrix} Y_{C,tar} & Y_{C,C_xH_y} & Y_{C,CH_4} & Y_{C,CO} & Y_{C,CO_2} & 0 & 0 \\ Y_{O,tar} & 0 & 0 & Y_{O,CO} & Y_{O,CO_2} & Y_{O,H_2O} & 0 \\ Y_{H,tar} & Y_{H,C_xH_y} & Y_{H,CH_4} & 0 & 0 & Y_{H,H_2O} & Y_{H,H_2} \\ 0 & 0 & 0 & -Y_{H_2,F}/Y_{CO,F} & 0 & 0 & 1 \\ 0 & 0 & -1 & 0.146 & 0 & 0 & 0 \\ LHV_G & LHV_{C_xH_y} & LHV_{CH_4} & LHV_{CO} & 0 & LHV_G & LHV_{H_2} \\ 0 & 0 & 0 & 0 & 0 & 0 & 1 \end{bmatrix} \begin{bmatrix} Y_{tar,F} \\ Y_{C_xH_y,F} \\ Y_{CH_4,F} \\ Y_{CO,F} \\ Y_{CO_2,F} \\ Y_{H_2O,F} \\ Y_{H_2,F} \end{bmatrix}$$
$$= \begin{bmatrix} Y_{C,F} - Y_{C,ch}Y_{ch,F} \\ Y_{O,F} - Y_{O.ch}Y_{ch,F} \\ Y_{H,F} - Y_{H,ch}Y_{ch,F} \\ 0 \\ 2.18 \cdot 10^{-4} \\ \left(\sum_j Y_{j,F} - Y_{ch,F}\sum_j Y_{j,ch}\right) LHV_{syn} \\ Y_{H_2,F} \end{bmatrix} \tag{3.67}$$

It is important to note that the calculation only takes into account the emissions coming from C, H, and O. The emission of compounds arising from N and S can be calculated directly, assuming that they form their corresponding reduced, gaseous products [34].

For the simplicity of modeling in the fluid and heat transport, the pyrolysis product model will be solved independently and then the bulk properties will be calculated. In the COMSOL model, the pyrolysis products are lumped into one species.

3.3.3.2 Eddy Break-Up Model

The Eddy Break-Up model uses variables calculated in the CFD module to define the combustion rates in the gaseous phase. The combustion rate is defined as follows [50]:

$$R_{comb} = \frac{\rho}{M_{syn}} \frac{\varepsilon}{k} \min\left\{ C_{r1} \min\left[x_{syn}, \frac{x_{O_2}}{\beta^{ST}} \right], C_{r2} \frac{x_{H_2O}}{1+\beta^{ST}} \right\} \tag{3.68}$$

3.3.4 Modeling the heat transport

The heat transport equation within the entire geometry is defined as follows [14]:

$$\rho c_p \vec{u} \cdot \nabla T = \nabla \cdot \left(k_p T\right) + Q + Q_p \tag{3.69}$$

In order to account for the heat energy emitted by the pile due to radiation, the following condition takes effect at the top of the pile:

$$-\vec{n} \cdot \left(-k_p \nabla T\right) = \epsilon\sigma \left(T_{amb}^4 - T^4\right) \tag{3.70}$$

The boundary conditions at the outlet and walls are defined as follows:

$$\vec{n} \cdot \left(-k_p \nabla T\right) = 0 \tag{3.71}$$

The boundary condition at the inlets is defined as follows:

$$T = T_0 \tag{3.72}$$

The heat from the reactions is defined using the reaction rates from the previous section, then multiplying by the corresponding heats of reaction:

$$Q_i = R_i \Delta h_{rxn,i} \tag{3.73}$$

The amount of latent heat absorbed or emitted due to convective heat transfer between the pellets and the pile is described as follows:

$$Q_p = sh\left(T_p - T\right) \tag{3.74}$$

3.3.5 Modeling the pollutant formation

The formation of pollutants, when considered dilute, is modeled as follows [14]:

$$\nabla \cdot \left(D_i \nabla c_i\right) + \vec{u} \cdot \nabla c_i = R_i \tag{3.75}$$

Most of the pollutant formation can be considered by means of generation from the pile (as calculated earlier). The formation of thermal NO_x occurs in the gaseous phase, and can be modeled given the following kinetic rate law [21]:

$$R_{NO_x} = \sqrt{\frac{3.6 \cdot 10^{37} K}{T}} \exp\left[-\frac{69090K}{T}\right] \left(\frac{c_{N_2}}{1^{mol/cm^3}}\right) \left(\frac{c_{O_2}}{1^{mol/cm^3}}\right)^{1/2} \frac{mol}{cm^3 \cdot s} \tag{3.76}$$

The boundary conditions at the walls is defined as follows:

$$\vec{n} \cdot (-D_i \nabla c_i + \vec{u} c_i) = 0 \tag{3.77}$$

The boundary conditions at the inlets are as follows, (assuming negligible pollutant concentration at the inlet):

$$c_i = 0 \tag{3.78}$$

The boundary condition at the outlet is as follows:

$$\vec{n} \cdot D_i \nabla c_i = 0 \tag{3.79}$$

3.3.6 Considerations on modeling in COMSOL

To solve the CFD problem, encompassing all of the differential equations listed above, the computational program COMSOL Multiphysics is used. COMSOL includes, built in, physical properties of the major gases in question. It also can compute the RANS problem without user input of k or ε values.

The burner geometry, including the zones of the pellet pile, are meshed into a discrete set of points. Extra fine meshing is used along boundaries of the pile and the walls touching the pile. When solving, the problem variables are segregated into four different groups in order to shorten the time per iteration. The entire study is also separated into three solving phases to improve the likelihood of convergence. First, the study is solved neglecting any reactions. The result of this study is used in the second phase as the initial guess. Next the reactions of the pile are included. In the third phase, the reactions in the gaseous phase are included as well.

The nonlinear solver uses the Newton method for calculating solutions. In order to populate the matrices to be solved in the iteration, a combination of the MUMPS and PARADISO methods are used [4].

3.4 Operational Parameters

The first trial to be simulated will be the, so-called, *base case*. The base case is a best estimation of the designed operation of the constructed prototype. In order to see how to improve operation, the following operating parameters will be varied:

- Flow rate of secondary air
- Trajectory of secondary air

- Addition of tertiary air jets

The following design modifications will also be considered:

- Moving the burner exit to the top
- Adding a sloped roof to increase residence time

Table 3.1: Simulations

Label	Description
Base	The base case intended to simulate the current design of the burner
DownSec	The same as Base but with the secondary air aimed downward by 25°
DownSecSlow	The same as DownSec but with the secondary air injection reduced by a factor of 3
DownSecSlope	The same as DownSec but with the roof sloped upward (from left to right)
DownSecSlopeJet	The same as DownSecSlope but with a tertiary air jet on the right wall below the outlet.
DownSecSlopeJetDown	The same as DownSecSlopeJet but with the tertiary jet pointed downward by 30°
Top	The same as Base but with the outlet moved to the top of the burner instead of the front
DownSecTop	The same as Top but with the secondary air aimed downward by 25°
DownSecSlowTop	The same as DownSecTop but with the secondary air injection reduced by a factor of 3
NoSec	The same as Base but with no secondary air

Chapter 4

Results and Discussion

In the following discussion of results, it is important to note that the main focus of the data is the *qualitative* trends displayed; not necessarily the specific values. Since the model depends on certain assumptions or approximations of reality, and since there is no experimental data on the prototype yet available, it is difficult to prove that all of the quantities calculated are extremely accurate. However, what the models will be able to do is provide insight on the qualitative trends. These trends depend on the underlying physics of the system, which have been extensively covered. The quantities, conversely, depend on the parameters and constants chosen.

4.1 Pellet Drying

For evaluating the drying of a pellet, the standard size of $6mm \times 25mm$ was chosen. Henceforth, it was assumed that the pellets (as received) have this uniform size and composition. The heat and mass balances were evaluated using a transient solver in COMSOL. The solution consisted of temperature and moisture content as functions of time and position (r and z in cylindrical coordinates).

Drying, as a mechanism, occurs due to the addition of heat to the pellet. In the simulation, it was assumed that the heat supplied to the pellet comes via convection with the surrounding air. The total moisture content, as a function of time, showed that there are three main stages to pellet drying.

For the first stage, the moisture content stays completely flat. During this stage, a heat flux occurs from the surrounding air to the pellet, due to the temperature difference. The temperature of the pellet rises until it reaches a point where the contained moisture can begin to evaporate.

In the second stage, once the evaporation begins, the moisture content decreases at a fairly constant rate. This stage constitutes approximately half of the evaporation of the pellet's total moisture. During this stage, the temperature within the pellet is

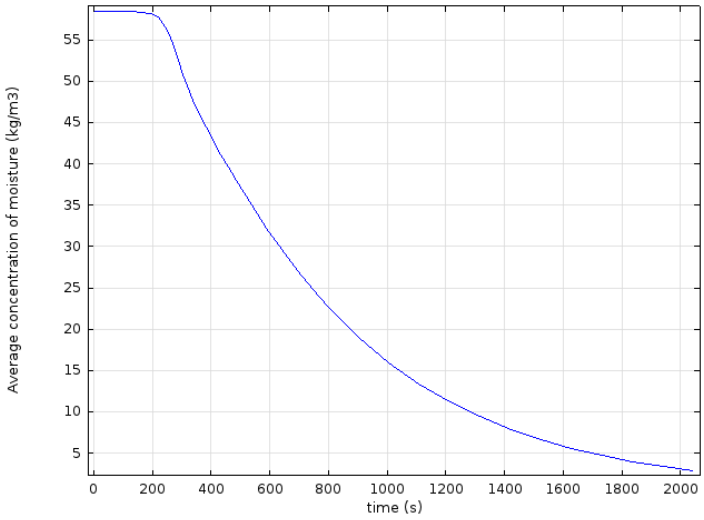

Figure 4.1: Average moisture content during drying

uniform and constant. A profile of moisture within the pellet forms. This profile, while decreasing in magnitude over time, displays a constant slope. In the sense of mass transport, this means that the flow of moisture from the inside to the outside has reached its equilibrium rate. It also clearly means that since the moisture content is decreasing at a constant rate, then the rate limiting mechanism during this stage is the traveling of water from the center of the pellet to the surface.

The third stage appears as the moisture content decrease is no longer linear, and resembles something closer to an exponential decay. In this stage, the internal moisture profile of the pellet is the same as the second stage: a linear slope with respect to distance. However, the moisture slope no longer reflects this, meaning that there is a new effect at the surface. The surface layer of water that typically forms when there is enough moisture in the pellet, cannot form now. Thus the vapor pressure of the water in the pellet decays (in a mathematical sense), evidenced by the decrease in the magnitude of the slope.

Using the concentration versus time data, the average pellet moisture content during the drying process was calculated to be $24 kg/m^3$ using equation 3.16.

The data also supports the earlier claim that the temperature profile within the pellet is relatively uniform compared to the moisture profile. In the simulation, the temperature reaches a uniform value on a scale of about 10 seconds while the moisture does not even on the order of hundreds of seconds. For this reason, for the proceeding calculations on the pile and system level, it was assumed that there was no temperature gradient within the pellets.

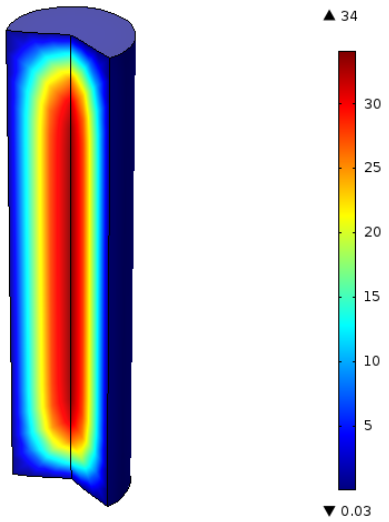

Figure 4.2: Moisture profile of a pellet while drying (kg/m^3)

4.2 Velocity Profiles

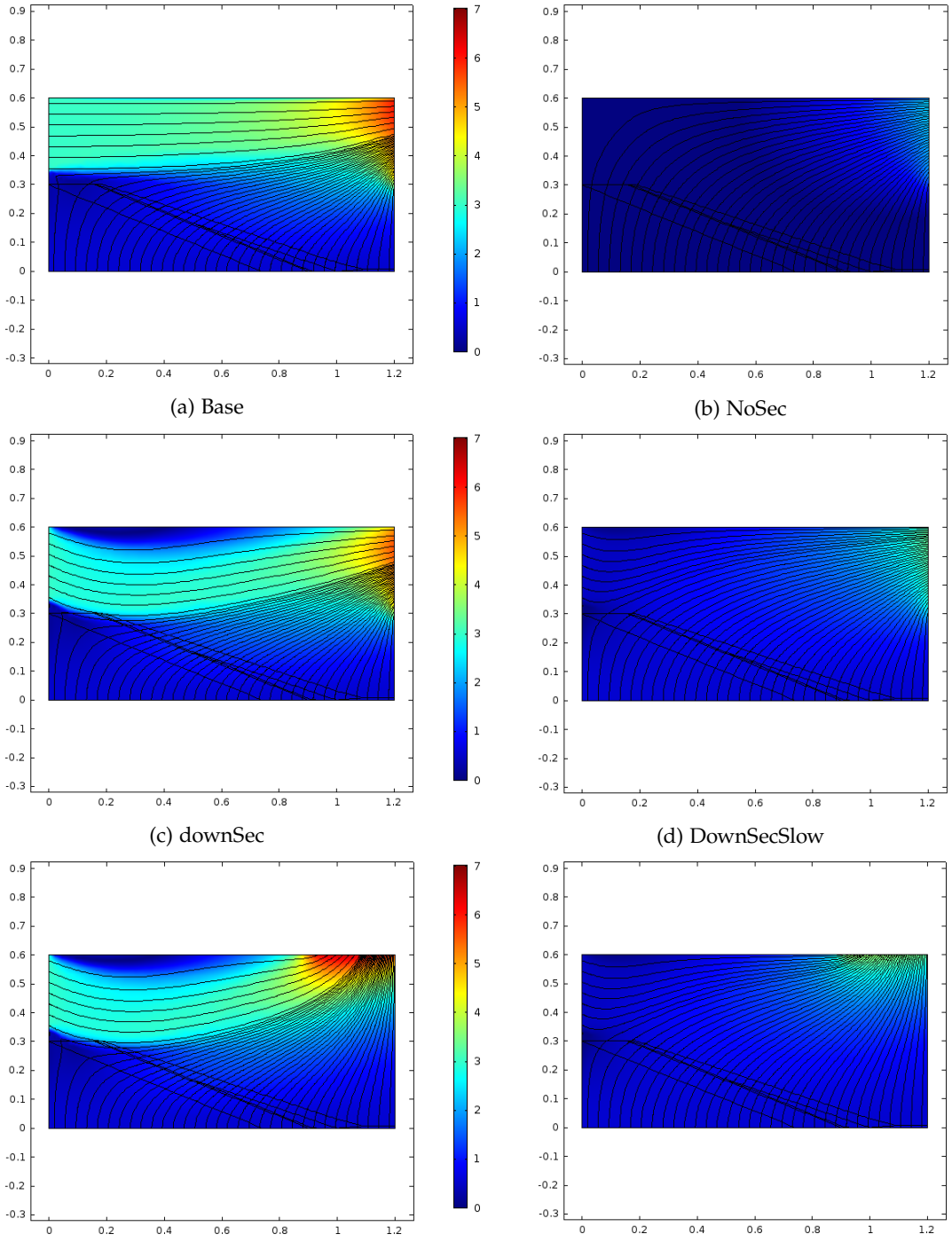

(a) Base (b) NoSec

(c) downSec (d) DownSecSlow

(e) DownSecTop (f) DownSecSlowTop

Figure 4.3: Velocity profiles (m/s)

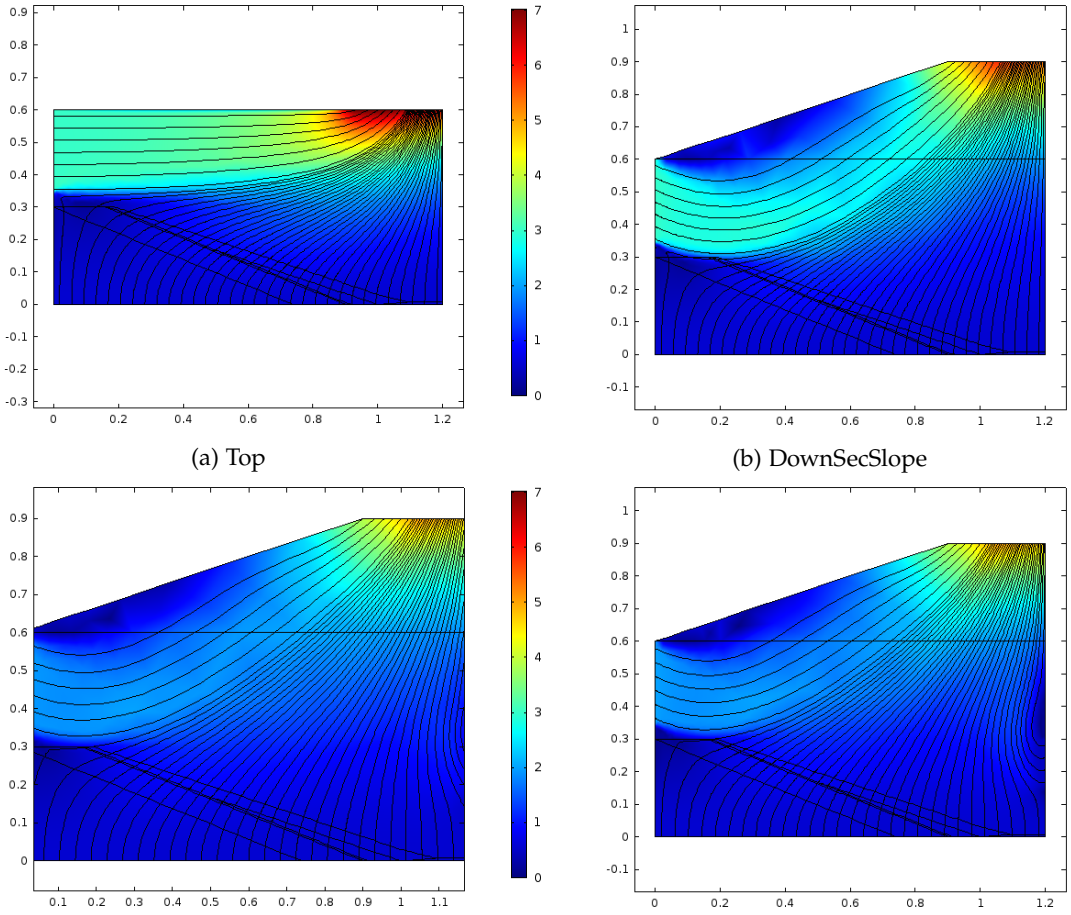

(a) Top

(b) DownSecSlope

(c) DownSecSlopeJet

(d) DownSecSlopeJetDown

Figure 4.4: Velocity profiles (m/s)

These velocity profiles come from the CFD problem defined in the previous chapter and solved in COMSOL.

4.3 Temperature profiles

There are two temperature profiles solved for in the model: the profile of the gas and the profile of the pellet pile. Over the course of many permutations of the operating parameters, several characteristics of the gas profile stand out clearly. The temperature is relatively low in many parts of the burner, and the maximum expected temperature observed is the adiabatic flame temperature of carbon (char), $\sim 1900°C$.

Under all conditions studied, the hottest part of the temperature profile of the gas occurs toward the end of the pile, after the wet and the dry pellets have been depleted and before a significant layer of bottom ash cumulates (see figure 4.5). In the base

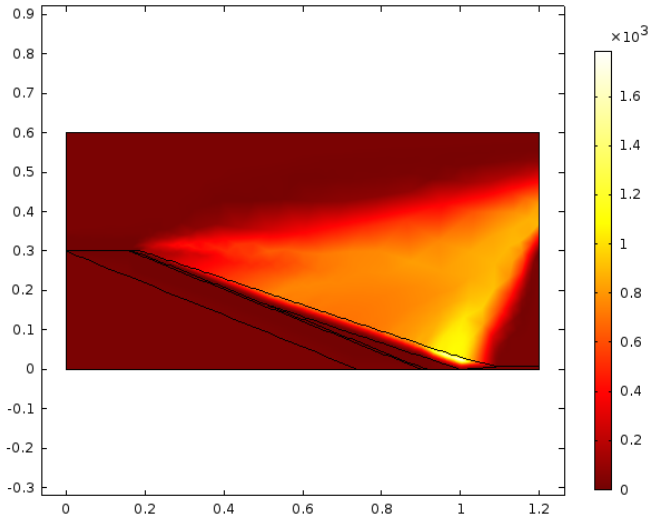

Figure 4.5: Temperature profile of Base ($^{\circ}C$)

case, meant to simulate the current operating conditions of the prototype, the hot spot at the end of the pile reaches a temperature of $1811^{\circ}C$.

Depending on the injection of secondary air and the positioning of the burner outlet, the shape of the temperature profile may change slightly, but the overwhelming trend is that there is a significant hotspot that forms at the end of the pile.

4.3.1 Hotspot Temperature

The conventional wisdom in the design of biomass burners is to avoid the formation of excessive hotspots within the burner chamber since this increases the kinetics for thermal NO_x generation (see equation 3.76). The overwhelming trend (in every simulation) showed that no matter the configuration of the burner or the secondary air injection, the hottest part of the burner always occurs toward the end of the pile where the wet and dry pellet zones disappear. At this point, the thickness of the char zone is at its maximum. Since it is the reaction within the char zone that has the highest heat of reaction by magnitude ($-32800^{kJ}/_{kg}$), it makes sense that that the temperature will be highest where the char zone is thickest. The temperature of the gases coming off the pile depends on the thickness of the char zone that they travel through. The longer the time in the zone, the hotter the temperature will be. So regardless of the configuration of the secondary air, there will always be a *hotter* spot occurring at this point in the pile.

While there will always be a hotspot, the temperature could feasibly be reduced if the rate of gases passing through it increases. This would mean less time to absorb heat. This principle could be expressed by a simple energy balance:

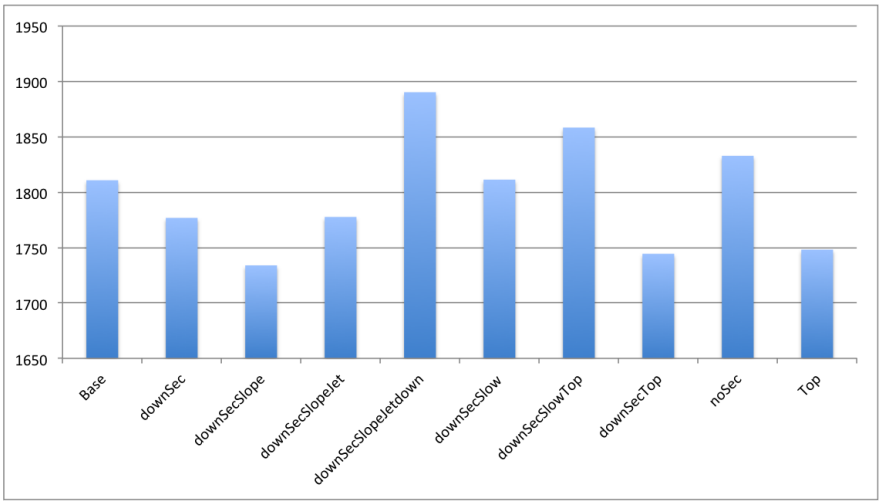

Figure 4.6: Hotspot Temperature ($^{\circ}C$)

$$\dot{Q} = \dot{m} c_p \Delta T \tag{4.1}$$

If the heat power, $\dot{Q}$ and the heat capacity, c_p, are considered constant, an increase in mass flow, $\dot{m}$, must imply a decrease in the temperature increase, ΔT.

With this in mind, the secondary air injection could limit this temperature by reducing the residence time of the passing air in the char combustion zone, thus reducing the amount of heat collected per mass of air. However, the results show that when the secondary air is pointed downward, there is really no significant effect on the hotspot temperature. As seen in the velocity profile (see figure 4.3c), even by pointing the secondary air downward, the air path is not really affected in the region of the hotspot. The main effect is at the beginning of the pile. Thus, with respect to the burner design in question, the direction alone can not affect the temperature.

One surprising effect was that the temperature of the hotspot decreased when the secondary air inlet was slowed. It was expected that this would increase since the residence of air would, feasibly, be longer. The velocity profile provides a slight insight (see figure 4.3d). Less secondary air means that the primary air has less force confining it downward, so the result is faster primary air from the bottom. The hotspot temperature decreased by more than $70^{\circ}C$.

When the position of the outlet was shifted from the front to the top, the effect was reversed. As the secondary air was slowed down, the hotspot temperature increases by about $120^{\circ}C$. Meanwhile, the direction does not appear to matter, but at higher secondary air flow, the hotspot temperatures are about $50^{\circ}C$ less. In this case, the velocity profile shows that the movement of the outlet to the top allows a more direct path for the primary air, explaining the decrease in the hotspot temperature.

The inclusion of tertiary jets near the hotspot also did not seem to improve the temperature, in fact the jets increased the temperature. This is most likely because they

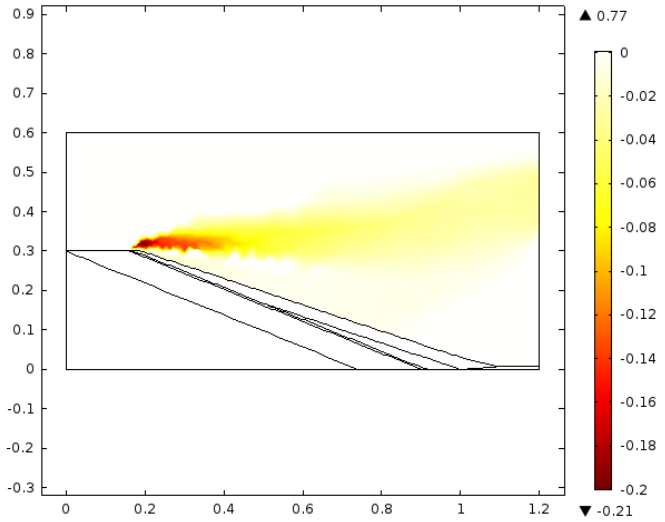

Figure 4.7: Consumption rate of pyrolysis gases ($kg/m^3 \cdot s$)

deflect more primary air toward the hotpot then they push it away (as shown in the velocity profile). Again, the deflection of air would effectively decrease the mass flow rate (see equation 4.1).

4.4 Variation of secondary air and outlet position with respect to boiler performance

While the rate of primary air remained fixed to allow as complete oxidation of the char as possible, the secondary air was varied in several different ways in order to study the effects on the operation of the burner. For example, in the base case, according to calculation, the amount of heat (enthalpy) exiting the burner outlet is $164 kW/m$ (on a per meter basis since the problem was solved in 2-D instead of three; the total outlet heat would be this value multiplied by the depth of the burner).

First, in an attempt to decrease the temperature at the hotspot, the secondary air trajectory was shifted downward toward it by 25°. As expected, the hotspot cooled slightly (by about 30°), but a more pronounced effect was that the outlet heat was reduced to $161 kW/m$. Since the amount of secondary air was unchanged, it was not dilution that reduced this heat rate. It was actually a reduction in the secondary combustion[1] taking place with the pyrolysis products. The model shows that the largest rate of pyro gas combustion occurs at the top of the pile. The aiming of the secondary air downward caused the residence time of the pyro gases to decrease, effectively pushing them toward the outlet faster.

[1] Gaseous combustion resulting from the reaction of pyrolysis gases with secondary air

Since this showed an adverse effect on the heat output, the amount of secondary air was decreased significantly with hopes of still reducing the hotspot temperature without decreasing the output heat. Surprisingly, the result was that the heat output dropped even further to $108^{kW}/_{m}$.

With each of these secondary air injection strategies, the outlet was also tried on the top of the burner instead of the front. According to the velocity profile, this leads to higher residence times virtually across the board. Since the secondary air has a less direct path to the outlet, more turbulence causes a slower exit. As a result, in the instances where the secondary air was at full capacity, this increased the heat output up to 30%.

In addition to the upward exit, a third construction variation was tried including a sloped roof. The slope caused a marked reduction in the output heat. Perhaps this is due to less mixing of the secondary air with the pyrolysis gases (see figure 4.4b).

4.5 Formation of pollutants

In the proceeding report, pollutant formation will be centered on *CO* and thermal NO_x. This is because the mechanisms governing their formation depend more on the CFD calculations than the other pollutants.

4.5.1 *CO*

The amount of *CO* emitted by the burner is a direct result of the residence time of the pyrolysis gases in the burner Hustad et al. [23]. If the gases exit too quickly, a significant portion of the *CO* remains unburned. It is possible for the secondary combustion to continue past the outlet if the temperature is high enough. In fact, the trials of the prototype showed the flame exiting out the front for at least an extra half-meter, as seen in figure 4.8. However, a flame outside the burning chamber could result in too much direct radiation on the heat exchangers.

In the cases where the secondary air was added at its base rate (horizontally or downward) the resulting *CO* emission varied only slightly. When the exit was moved to the top, there was a clear reduction in the *CO* due to greater residence time. However, in the case where the downward secondary air was slower, the front exit burner showed a 20% increase and the top exit burner showed nearly a 50% increase in *CO* emissions.

Figure 4.8: Actual burner in operation

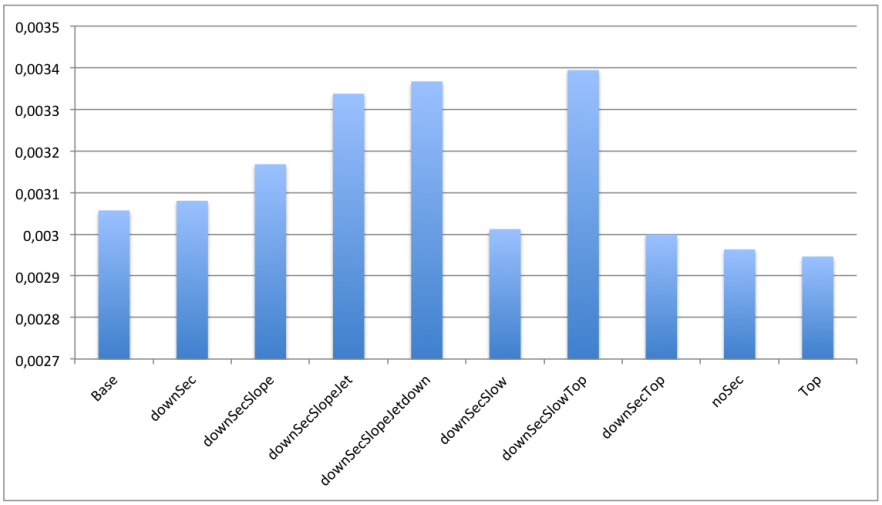

Figure 4.9: Emission of CO ($kg/m{\cdot}s$)

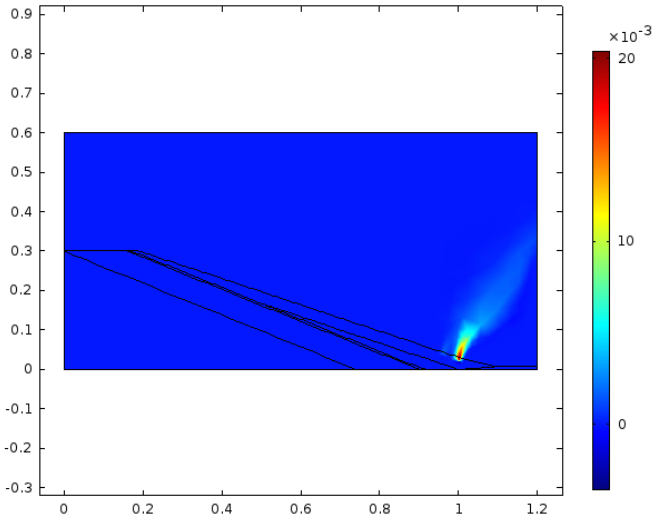

Figure 4.10: NO_x concentration profile ($^{mol}/_{m^3}$)

4.5.2 Thermal NO_x

In order to validate the model, it is first important to verify that it can predict well known behavior: namely, that the inclusion of air staging reduces NO_x emissions. So the model was both run in a condition with no secondary air, and the base condition of secondary air. By including the secondary air, the NO_x emission was reduced by more than three times. So the trends of the model at least are able to emulate the well established realities.

In the base case, the emission of NO_x was calculated to be $2.51^{mol}/_{m \cdot s}$. The first attempt to reduce this number was through reducing the hot spot temperature, by aiming the secondary air downward. This led to a 25% decrease in the amount of NO_x. When the downward air was slowed in an attempt to raise the residence time, the NO_x emission rates returned to around the same value as the base case. Another possibility of how this reduced the NO_x emission is by redirecting the oxygen-lean, post-combustion air back toward the hotspot.

In a second attempt to increase residence time, when the burner outlet was moved to the top, the cases where the secondary air rate was fixed showed mixed results. However, in the case of the slowed downward secondary air, the amount of NO_x jumped by more than three times compared to the case where the exit was in the front. The addition of the sloping roof also showed an increase in NO_x production.

One additional technique attempting to reduce the NO_x emissions by reducing the hotspot temperature was introducing a small tertiary air jet aimed either above or directly at the hotspot. Instead of decreasing the emissions, the inclusion of this air jet increases them. When aimed above the hotspot, it increases the emission by a

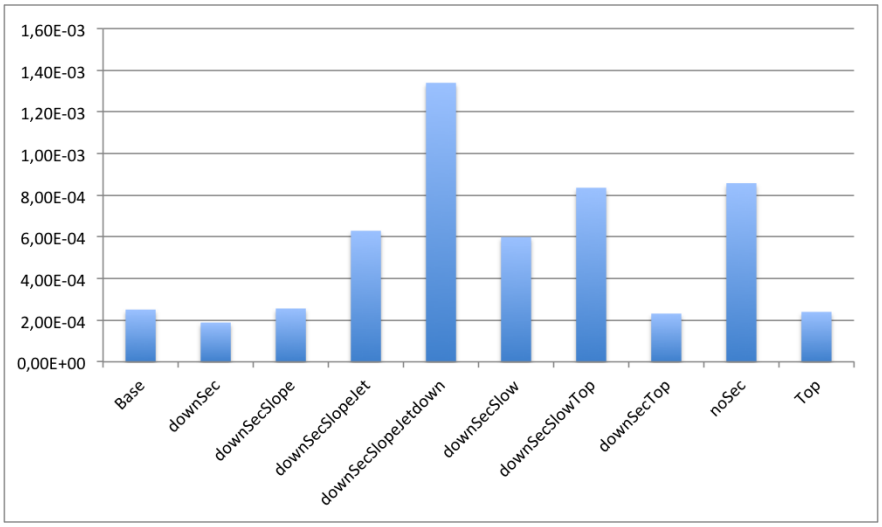

Figure 4.11: Emission of NO_x ($kg/m \cdot s$)

factor of two. When aimed directly at the hotspot, it increases emissions by a factor of five. This result means that there is clearly a narrow optimum in the amount of secondary or tertiary air that should be directed toward the hotspot. While it does decrease the temperature, it is clear that introducing extra N_2 and O_2 at this site makes the reaction faster more than reducing the temperature makes it slower. The optimization should be done on a case to case basis depending on the burner design.

4.6 Profiles exiting the burner chamber

As expected (based on experiments), the profiles of energy and heat at the burner outlet are seldom uniform. Since the dynamics within the burner affect the profile at the outlet, it is feasible to believe that changing the operating parameters could change the exiting profile.

For example, in the base case, the heat flux profile at the exit reflects both theory and practice. The peak of the heat occurs slightly above the bottom of the outlet. This coincides with the actual operation of the burner where the flames are clearly visible exiting at lower end (see figure 4.8). In the case where the exit of the burner is on top, this only varies slightly, with the peak still occurring toward the further end of the burner. Based on the simulations run, it appears that there is very little opportunity to vary the heat profile exiting the burner.

4.7 Design strategies for future considerations

Based on the results catalogued above, there are several clear design strategies that should be taken into account in the future:

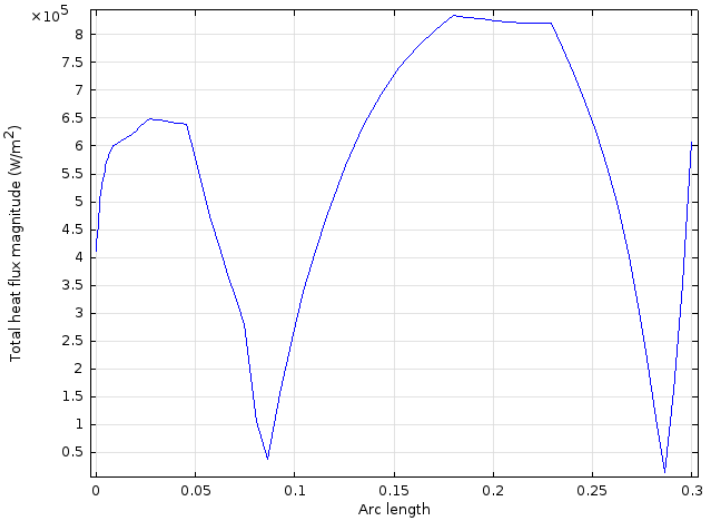

Figure 4.12: Heat flux profile of burner outlet for Base

- Increase the mass flow of air through the hotspot to reduce the hotspot temperature
  - achieved by reducing secondary overflow
  - also achieved by moving the burner outlet to the top
- Increase the total residence time in the burner to increase CO conversion
  - achieved by moving burner outlet to the top
  - in some cases, improved by reducing secondary flow
- Do *not* include tertiary jets near the hotspot
- Reduce oxygen present in the hotspot to decrease NO_x production
  - achieved by redirecting secondary air downward
- No sloping roof

Chapter 5

Conclusion

In the preceding report, CFD was used to analyse the effects that different design and operating parameters have on the performance and pollutant production in an existing grate burner design. The design, created by the Departamento de Ingeniería Mecánica at the Universidad Politécnica de Madrid, is a biomass pellet burner intended for district and residential heating applications. The burner consists of a main combustion chamber and an antechamber. It is fed with pellets through feed tubes and fed with primary air and secondary air via two large fans entering the antechamber. The goal of this report was to take the existing design and suggest modifications that would improve it.

A comprehensive model of the pellet burner was created, consisting of three different scales: the pellet scale, the pellet-pile scale, and the entire-burner scale. On the pellet scale, the kinetics of drying were analysed in order to characterise the drying profile of the pellets. Using this analysis, the drying profile was applied to the pellet-pile scale, assuming evaporation and inert zones. An existing pellet pile profile based on previous experiments was incorporated in order to simplify the pile model into a series of mass balances. Using the results of these mass balances, the emissions from the pile where incorporated into the burner chamber model.

The results from the model showed that there is room for improvement in the burner design, with respect to pollutant emissions. The current design with a flue gas outlet in the front and a secondary air flow blowing horizontally over the pile does not represent the optimal operation. In order to improve the emissions of NO_x, the secondary air flow can be redirected more downward and slightly reduced. In order to increase the conversion of CO to CO_2, the outlet of the burner can be moved from the front to the top.

With these and other considerations, the design of the burner will be altered, but the research at Universidad Politécnica de Madrid is ongoing. Soon, data will be collected on the heat output and the emission levels from the burner. When this happens, it will be cross-referenced with this model so that the parameters chosen within the model can be properly calibrated.

There are other operational issues to be concerned about including jamming of the screws, proper collection of the bottom ash, incorporation of an Archemides-screw pellet feeder for more consistent fuel inlet, etc. The current prototype is not yet capable of working in a completely continuous fashion. Incorporation of the suggestions from this report and the other mechanical modifications will, hopefully, allow a more efficient operation. The next prototype design is currently being constructed, and once it is capable of continuous operation, it will be coupled with a boiler for more experimentation.

Appendix A

MATLAB Code

```
% Anthony Durbano
%
% This code uses parameters observed in the profile of a pellet pile to
% calculate the reaction rates.

function pileSolver

% Wet Zone

vPile=.001;                             %velocity of the pile (m/s)
tEva0=160;                              %time of wet zone first shriking (s)
tEvaf=900;                              %time of wet zone disappearing (s)
h0=.3;                                  %inital height of the pile (m)
vZ=h0/(tEvaf-tEva0);                    %velocity of the evaporation zone (m/s)
lZ=vZ*tEva0;                            %length of evaporation zone (m)
c0=35.1;                                %initial concentration of water (kg/m3)
cZ=24;                                  %concentration of water
                                        %   in evaporation zone (kg/m3)
t=0:1200;                               %time window (s)
Lz=(ones(size(t))*lZ-(t<tEva0)...
    .*(tEva0-t)*vZ-(t>(tEvaf-...
    tEva0)).*(t-tEvaf+tEva0)*...
    vZ).*(t<tEvaf);                     %variable length of evap zone (m)
Li=(h0-t*vZ).*~(t>(tEvaf-...
    tEva0))+(t>(tEvaf-tEva0))*0;        %variable length of inert zone (m)
m=c0*Li+cZ*Lz;                          %total mass of water per area (kg/m2)
J=-diff(m)./diff(t);                    %flux of water (kg/m2/s)
hw=Lz+Li;                               %height of the wet zone (m)
Jw=interp1(t(2:end)-.5,J,t,...
    'linear','extrap')./Lz;             %reaction rate of the wet
                                        %   zone (kg/m3/s)
hL=h0-hw;                               %height "outlet" (m)
```

```
% Dry Zone

cVol=388.59;                          %concentration of volatile
                                      %   material (kg/m3)
hSS=.005;                             %thickness of steady state dry zone (m)
dhIn=diff(hL)./diff(t);               %height "inlet" rate (m/s)
k=vZ/hSS;                             %pyrolysis first order kinetic
                                      %   coefficient (1/s)
[~,hd]=ode23(@diffeq1,t,0);
    function dy=diffeq1(time,y)
       dy=interp1(t(2:end)-.5,...
       dhIn,time,'linear',...
       'extrap')-k*y;                 %height "balance" (m/s)
    end
hd=hd';                               %height of dry zone (m)
Jv=k*hd*cVol./hd;                     %reaction rate of dry zone (kg/m3/s)
hL=h0-hw-hd;                          %height "outlet" (m)

% Char Zone

cC=84.68;                             %concentration of fixed carbon (kg/m3)
dhIn=diff(hL)./diff(t);               %height "inlet" rate (m/s)
dhBurn=vZ-.08/1100;                   %char burning height rate (m/s)
[~,hc]=ode23(@diffeq2,t,0);
    function dy=diffeq2(time,~)
       dy=interp1(t(2:end)-.5,...
       dhIn,time,'linear',...
       'extrap')-dhBurn*(time>190);    %height "balance" (m/s)
    end
hc=(hc.*(hc>0))';                     %height of the char zone (m)
Jc=dhBurn.*(t>190)*cC.*(hc>0)./hc;    %reaction rate of char zone (kg/m3/s)
hL=h0-hw-hd-hc;                       %height "outlet" (m)

% Ash Zone

cA=1196.6;                            %concentration of ash (kg/m3)
dhIn=diff(hL)./diff(t);               %height "inlet" rate (m/s)
f=7/30;                               %height tuning factor
[~,ha]=ode23(@diffeq3,t,0);
    function dy=diffeq3(time,~)
       dy=interp1(t(2:end)-.5,...
       dhIn,time,'linear',...
```

```
       'extrap')*f*(time>1000);     %height "balance" (m/s)
    end
ha=(ha.*(ha>0))';                   %height of ash zone (m)

% Data output

x=t'*vPile;                         %horizontal axis (m)
hEach=[ha;ha+hw-Lz;ha+hw;...
    ha+hw+hd;ha+hw+hd+hc]';         %height profile (m)

hEach=round(hEach,4);
reg=find(hEach(:,1)~=0);
reg=[reg(1)-1;reg;reg(end)+1];
if reg(1)==0, reg=reg(2:end); end
if reg(end)==numel(x)+1, reg=reg(1:end-1); end
csvwrite('DataOut/BotAsh.csv',[x(reg),hEach(reg,1)])
reg=find(hEach(:,2)~=hEach(:,1));
reg=[reg(1)-1;reg;reg(end)+1];
if reg(1)==0, reg=reg(2:end); end
if reg(end)==numel(x)+1, reg=reg(1:end-1); end
csvwrite('DataOut/WetRxn.csv',[x(reg),hEach(reg,2)])
csvwrite('DataOut/WetFlux.csv',[x(reg),Jw(reg)'])
reg=find(hEach(:,3)~=hEach(:,2));
reg=[reg(1)-1;reg;reg(end)+1];
if reg(1)==0, reg=reg(2:end); end
if reg(end)==numel(x)+1, reg=reg(1:end-1); end
csvwrite('DataOut/Wet.csv',[x(reg),hEach(reg,3)])
reg=find(hEach(:,4)~=hEach(:,3));
reg=[reg(1)-1;reg;reg(end)+1];
if reg(1)==0, reg=reg(2:end); end
if reg(end)==numel(x)+1, reg=reg(1:end-1); end
csvwrite('DataOut/Dry.csv',[x(reg),hEach(reg,4)])
csvwrite('DataOut/VolFlux.csv',[x(reg),Jv(reg)'])
reg=find(hEach(:,5)~=hEach(:,4));
reg=[reg(1)-1;reg;reg(end)+1];
if reg(1)==0, reg=reg(2:end); end
if reg(end)==numel(x)+1, reg=reg(1:end-1); end
csvwrite('DataOut/Char.csv',[x(reg),hEach(reg,5)])
csvwrite('DataOut/CharFlux.csv',[x(reg),Jc(reg)'])

end
```

Nomenclature

B.1 Latin Alphabet

Symbol	Unit (MKS)	Description
a	$1/s$	Parabolic PDE coefficient
A^*	-	Antoine parameter for H_2O
A_x	m^2	Cross-sectional area
B^*	K	Antoine parameter for H_2O
Bi	-	Biot number
c	m^2/s	Parabolic PDE coefficient
c_i	kg/m^3 or mol/m^3	Concentration of species i
c_p	$J/kg \cdot K$	Specific heat capacity
C^*	K	Antoine parameter for H_2O
$C_{\varepsilon 1}$,$C_{\varepsilon 2}$,C_μ	-	k-ε model parameter
C_{r1},C_{r2}	-	Eddy break-up parameter
d	m	Diameter of pellet
D_{ik}	m^2/s	Diffusion coefficient of species i through k
D^{eff}	m^2/s	Effective diffusion coefficient of water in pellet
E_r	J/mol	Activation energy of reaction r
f	m/s^2	PDE forcing function
g	m/s^2	Acceleration due to gravity
h	$W/m^2 \cdot K$	Heat transfer coefficient
h_d^{SS}	m	Steady state height of the dry zone
h_z	m	Height of zone z
$\dot{h}_{comb}$	m/s	Rate of height change due to combustion
$\dot{h}_{in,z}$	m/s	Rate of height entering zone z
i	-	Malmquist parameter
I	-	Identity matrix
I_T	-	Turbulence intensity
$\vec{j}_i$	$kg/m^2 \cdot s$ or $kg/m^2 \cdot s$	Flux of species i
k	m^2/s^2	Specific kinetic energy
k_M	$m/s \cdot Pa$	Mass transfer coefficient of moisture

Symbol	Unit (MKS)	Description
k_p	$W/m \cdot K$	Conductivity of pellet
k_z	$1/s$	Kinetic rate constant of reaction in zone z
ℓ	m	Characteristic length of pellet
L	m	Length of pellet
L_I	m	Length of inert zone
L_T	m	Turbulence length scale
L_Z	m	Length of evaporation zone
LHV_i	J/kg	Lower heating value of species i
$\dot{m}$	kg/s	Mass flow rate
m_i	kg	Mass of species i
m_s	-	Malmquist parameter
M_i	kg/mol	Molar mass of species i
n	-	Malmquist parameter
$\vec{n}$	-	Normal vector
p	Pa	Pressure
p_{H_2O}	Pa	Partial pressure of H_2O
$p^*_{H_2O}$	Pa	Vapor pressure of water
p^*_M	Pa	Vapor pressure of moisture in pellet
$\dot{Q}$	W	Heat power
Q_p	W/m^3	Heat power from pellet pile
Q_z	W/m^3	Heat power from zone z
r	m	Radial coordinate
R_i	$kg/m^3 \cdot s$ or $mol/m^3 \cdot s$	Production rate of species i
R_{IG}	$J/mol \cdot K$	Ideal gas constant
R_p	m	Pellet radius
s	$1/m$	Specific area (per volume)
Sc	-	Schmidt number
t	s	Time
t_{ev1},t_{ev2}	s	Time parameters for wet zone
T	K	Temperature
T_{amb}	K	Ambient temperature
T_p	K	Pellet temperature
$\vec{u}$	m/s	Velocity vector
$\vec{u}'$	m/s	Velocity turbulent fluctuations (RANS)
u_p	m/s	Velocity of pellet pile
u_s	m/s	Slip velocity
u_t	m/s	Terminal velocity
$\vec{u}_{tan}$	m/s	Tangential velocity
u_τ	m/s	Friction velocity
u_z	m/s	Velocity of evaporation zone
$\vec{U}$	m/s	Mean velocity (RANS)
V	m^3	Volume of pellet

Symbol	Unit (MKS)	Description
x	m	Horizontal coordinate
x_i	-	Mole fraction of species i
X	-	Arbitrary intensive material property
$Y_{i,k}$	-	Mass fraction of species i in k
z	m	Height coordinate

B.2 Greek Alphabet

Symbol	Unit (MKS)	Description
α^{ST}	-	Stoichiometric air/fuel ratio (by mass)
$\alpha^{ST}_{O_2}$	-	Stoichiometric O_2/fuel ratio (by mass)
β	-	Air/fuel ratio (by moles)
δ^+_w	-	Wall liftoff
$\Delta h_{rxn,i}$	J/kg	Heat of reaction for production of species i
ϵ	-	Emissivity of pile
ε	-	Dissipation
κ_v	Pa	Average viscous stress
λ	-	Equivalence ratio
μ	$Pa \cdot s$	Dynamic viscosity
ϕ	-	Porosity of pellet pile
ρ	kg/m^3	Density
ρ_i	kg/m^3	Density of species i
σ	$W/m^2 \cdot K^4$	Stefan-Boltzmann constant
σ_k	-	k-ε model parameter
θ_p	-	Effective volume fraction of water in pellet

B.3 Subscripts, superscripts, and symbol marks

Symbol	Description
0	inlet value
a	ash
air	air
amb	ambient
ba	bottom ash
c	char
$comb$	combustion
C	carbon
CO_2	carbon dioxide
d	dry

Symbol	Description
ev	evaporation
f	final
fa	fly ash
F	fuel
H	hydrogen
H_2O	water
i	species
k	species
M	moisture
N	nitrogen
N_2	nitrogen gas
O	oxygen
O_2	oxygen gas
p	pellet
P	product
ST	stoichiometric value
syn	pyrolysis gases
S	sulphur
v	pyrolysis gases
z	zone
Z	evaporation zone
$\bar{\bigcirc}$	average value
$\vec{\bigcirc}$	vector
$\bigcirc'$	DAF basis
$\dot{\bigcirc}$	rate

References

1. 2010. *Annual Energy Review 2009*. U.S. Energy Information Administration, Washington, DC. xiii, 2, 3

2. 2011. Methane. Technical report, National Institute of Standards and Techology. 11

3. 2011. Water. Technical report, National Institute of Standards and Techology. 30

4. 2013. *CFD Module User's Guide*. COMSOL. 38, 39, 43

5. 2015. http://ec.europa.eu/clima/policies/package/index_en.htm. 1

6. 2015. http://www.energy.gov/ne/nuclear-reactor-technologies. 2

7. 2015. http://www.world-nuclear.org/info/Facts-and-Figures/Nuclear-generation-by-country. 2

8. 2015. *Inventory of U.S. Greenhouse Gas Emissions and Sinks: 1990 – 2013*. EPA. xiii, 1, 2

9. Altay, H. M., 2009. *Physics-Based Flame Dynamics Modeling and Thermoacoustic Instability Mitigation*. Ph.D. thesis, Massachusetts Institute of Technology. 20

10. Bakker, A., 2005. Modeling chemical reactions with cfd: Reacting flows. (2005). 23

11. Bastías, M. V. and Cloutier, A., 2005. Evaluation of wood sorption models for high temperatures. *Maderas: Ciencia y Tecnología*, 7, 3 (2005), 145–58. 13, 29, 30

12. Bauer, R.; Gölles, M.; Brunner, T.; et al., 2010. Modelling of grate combustion in a medium scale biomass furnace for control purposes. *Biomass and Bioenergy*, 34 (2010), 417–27. 12

13. Boman, C., 2005. *Particulate and gaseous emissions from residential biomass combustion*. Dissertation, Umeå University, Energy Technology and Thermal Process Chemistry Umeå University SE-901 87 Umeå, Sweden. xiii, 6, 15, 20, 21, 22

14. Deen, W. E. I., 1998. *Analysis of Transport Phenomena*. Oxford University Press, 2nd edition edn. 28, 29, 41, 42

15. Demirbas, A., 2004. Combustion characteristics of different biomass fuels. *Progress in Energy and Combustion Science*, 30 (October 2004), 219–30. 7, 15

16. Demirbas, A., 2005. Potential applications of renewable energy sources, biomass combustion problems in boiler power systems and combustion related environmental issues. *Progress in Energy and Combustion Science*, 31 (February 2005), 171–92. 12

17. French, C., 2001. *Plant Engineer's Handbook*. Butterworth-Heinemann, 1st edition edn. xiii, 17, 18

18. Gupta, H., 2002. The effect of operating parameters on the selectivity of the carbon-no reaction in an oxidizing atmosphere. *Fuel and Energy Abstracts*, 43, 4 (2002), 291. 19

19. Hansen, J.; Kharecha, P.; Sato, M.; et al., 2013. Assessing "dangerous climate change": Required reduction of carbon emissions to protect young people, future generations and nature. *PLOS ONE*, 8, 12 (December 2013). xiii, 4

20. Heschel, W.; Rweyemamu, L.; Scheibner, T.; and Meyer, B., 1999. Abatement of emissions in small-scale combustors through utilisation of blended pellet fuels. *Fuel Processing Technology*, 61 (1999), 223–42. 16

21. Hesselmann, G. and Rivas, M., 2001. What are the main nox formation processes in combustion plant? *IFRF Online Combustion Handbook*, (December 2001). 42

22. Holloway, M. D.; Nwaoha, C.; and Onyewuenyi, O. A., 2012. *Process Plant Equipment: Operation, Control, and Reliability*. John Wiley and Sons. 19

23. Hustad, J. E.; Skreiberg, Ø.; and Sønju, O. K., 1995. Biomass combustion research and utilization in iea countries. *Biomass and Bioenergy*, 9, 1-5 (1995), 235–55. 6, 16, 17, 37, 53

24. Jenkins, B. M.; Baxter, L. L.; Miles Jr., T. R.; and Miles, T. R., 1998. Combustion properties of biomass. *Fuel Processing Technology*, 54 (1998), 17–46. 19

25. Khan, A.; de Jong, W.; Jansens, P.; and Spliethoff, H., 2009. Biomass combustion in fluidized bed boilers: Potential problems and remedies. *Fuel Processing Technology*, 90 (2009), 21–50. 9, 11, 16

26. Lautenberger, C. and Fernandez-Pello, C., 2009. Generalized pyrolysis model for combustible solids. *Fire Safety Journal*, 44 (2009), 819–39. 30, 32

27. Layokun, S. K. and Slater, D. H., 1979. Mechanism and kinetics of propane pyrolysis. *Industrial Engineering Chemical Process Design Development*, 18, 2 (April 1979), 232–36. 14

28. Lin, Y.-C.; Cho, J.; Tompsett, G. A.; et al., 2009. Kinetics and mechanism of cellulose pyrolysis. *Physical Chemistry*, 113 (2009), 20097–107. 15

29. Mafakheri, F. and Nasiri, F., 2014. Modeling of biomass-to-energy supply chain operations: Applications, challenges and research directions. *Energy Policy*, 67 (2014), 116–26. 6

30. Marinos-Kouris, D. and Maroulis, Z. B., 2006. *Handbook of Industrial Drying*. CRC Press, 3rd edition edn. xiii, 13, 14, 30

31. McAuley, S., 2014. Get to know your electricity bill, one line item at a time. EnerNOC, Inc. 3

32. McCarl, B. A.; Adams, D. M.; Alig, R. J.; and Chmelik, J. T., 2000. Competitiveness of biomass-fueled electrical power plants. *Annals of Operations Research*, 94 (2000), 37–55. 4

33. Miller, B. G. and Tillman, D., 2008. *Combustion Engineering Issues for Solid Fuel Systems*. Academic Press, 1st edition edn. 14, 21

34. Neves, D.; Thunman, H.; Matos, A.; et al., 2011. Characterization and prediction of biomass pyrolysis products. *Progress in Energy and Combustion Science*, 37 (2011), 611–30. 13, 15, 20, 40, 41

35. Newman, C., 2014. Primary and secondary combustion air and combustion gases. http://5at.co.uk/index.php/definitions/terrms-and-definitions/combustion-air.html. 20

36. Obernberger, I., 1998. Decentralized biomass combustion: state of the art and future development. *Biomass and Bioenergy*, 14, 1 (June 1998), 35–56. 3, 5, 7

37. Ramaswamy, S.; Huang, H.; and Ramarao, B., 2013. *Separation and Purification Technologies in Biorefineries*. John Wiley and Sons. 32, 33, 34

38. Rhén, C.; Öhman, M.; Gref, R.; et al., 2007. Effect of raw material composition in woody biomass pellets on combustion characteristics. *Biomass and Bioenergy*, 31 (2007), 66–72. 16

39. Rice, R. G. and Do, D. D., 1995. *Applied Mathematics and Modeling for Chemical Engineers*. John Wiley and Sons. 23, 24, 25

40. Roy, M. M.; Dutta, A.; and Corscadden, K., 2013. An experimental study of combustion and emissions of biomass pellets in a prototype pellet furnace. *Applied Energy*, 108 (2013), 298–307. 16

41. Saastamoinen, J.; Aho, M.; Moilanen, A.; et al., 2010. Burnout of pulverized biomass particles in large scale boiler – single particle model approach. *Biomass and Bioenergy*, 34 (2010), 728–36. 12, 16, 30, 31

42. Saastamoinen, J. J.; Taipale, R.; Horttanainen, M.; and Sarkomaa, P., 2000. Propagation of the ignition front in beds of wood particles. *Combustion and Flame*, 123, 1 (2000), 214–26. 32

43. Schaschke, C., 2014. *A Dictionary of Chemical Engineering*. Oxford University Press. 19

44. Schnelle Jr., K. B. and Brown, C. A., 2001. *Air Pollution Control Technology Handbook*. Handbook Series for Mechanical Engineering. CRC Press. 19

45. Sørensen, B., 2004. *Renewable Energy*. Academic Press. 2, 4

46. Speakes, K., 2004. Dispersed generation. *Power Economics*, 8, 2 (February 2004), 12. 3

47. Stearns, P. N., 2006. *The Industrial Revolution in World History*. Westview Press, 3rd edition edn. 4

48. Thunman, H. and Leckner, B., 2003. Co-current and counter-current fixed bed combustion of biofuel—a comparison. *Fuel*, 82 (2003), 275–83. xiii, 12, 15, 16, 22, 28, 32, 33

49. Tillman, D. A., 2000. Biomass cofiring: the technology, the experience, the combustion consequences. *Biomass and Bioenergy*, 19 (June 2000), 365–84. 5, 12

50. Tryggvason, G., 2001. *Classical Turbulence Modeling*. 24, 25, 41

51. van der Lans, R. P.; Pedersen, L.; Jensen, A.; et al., 2000. Modelling and experiments of straw combustion in a grate furnace. *Biomass and Bioenergy*, 19 (2000), 199–208. 32

52. Vassilev, S. V.; Baxter, D.; Andersen, L. K.; et al., 2012. An overview of the organic and inorganic phase composition of biomass. *Fuel*, 94 (2012), 1–33. 12

53. Wang, L.; Weller, C. L.; Jones, D. D.; and Hanna, M. A., 2008. Contemporary issues in thermal gasification of biomass and its application to electricity and fuel production. *Biomass and Bioenergy*, 32, 7 (573-81 2008). 19

54. Williams, A.; Jones, J. M.; Ma, L.; and Pourkashanian, M., 2012. Pollutants from the combustion of solid biomass fuels. *Progress in Energy and Combustion Science*, 38 (2012), 113–37. 20, 21, 22

55. Wrigley, E. A., 1988. *Continuity, chance and change: the character of the industrial revolution in England*. Cambridge University Press. 4

56. Yeboah, N. N.; Shearer, C. R.; Burns, S. E.; and Kurtis, K. E., 2014. Characterization of biomass and high carbon content coal ash for productive reuse applications. *Fuel*, 116 (January 2014), 438–47. 5

57. Zabetta, E. C.; Hupa, M.; and Saviharju, K., 2005. Reducing nox emissions using fuel staging, air staging, and selective noncatalytic reduction in synergy. *Industrial Engineering Chemistry Research*, 44 (2005), 4552–61. 18, 19